POLITECNICO
MILANO 1863

SCUOLA DI INGEGNERIA INDUSTRIALE
E DELL'INFORMAZIONE

Methodology for the determination of the K_{ISCC} for rock anchors materials in marine environment

TESI DI LAUREA MAGISTRALE IN
MATERIALS ENGINEERING AND NANOTECHNOLOGY-
INGEGNERIA DEI MATERIALI E DELLE NANOTECNOLOGIE

Author: **Giuseppe Caristo**

Student ID: 928041
Advisor: Ing. Andrea Gruttadauria
Co-advisor: Ing. João Teixeira Oliveira de Menezes
Academic Year: 2020-21

Abstract

Austenitic stainless steel are widely used for rock anchors in marine environment for rock climbing as well as for mining installation. The presence of chlorides in the atmosphere, the stresses induced by tightening and the susceptibility of the material to stress corrosion cracking (SCC) have led to numerous anchors failures. The aim of this work is to propose a useful methodology for deriving the Stress Corrosion Cracking susceptibility starting by the analysis of the tests described in the UIAA Standard (ASTM G36 and ASTM B117). The UIAA proposes two standards for the evaluation of the corrosion resistance which however do not consider the presence of a crack that can change the resistance. Crack that derives from the pitting of the component for countless reasons [1]. To remedy this, it is proposed to follow the fracture rules and therefore evaluate the K_{EAC}. To determine the effectiveness of the methodology, samples were prepared in three different materials (proposed by UIAA as candidates for the application), AISI 316L, SAF2205, Titanium Grade 5 and then the test was prepared. The test after thirty days showed that the materials are still good for their application. Furthermore, the technique proves to be reliable and allows to obtain more information on the degradation rate, on the times and on the applied loads.

Key-words: Stress Corrosion Cracking; Rock anchors; Stainless steel; Titanium; Fracture toughness; crack propagation.

Abstract in lingua italiana

Gli ancoraggi in acciaio inossidabile austenitico sono ampiamente utilizzati come ancoraggi da roccia nell'ambiente marino per l'arrampicata su roccia e per l'installazione mineraria. La presenza di cloruri nell'atmosfera, le sollecitazioni indotte dal serraggio e la suscettibilità del materiale alla tensocorrosione (SCC) hanno determinato la rottura di numerosi ancoranti. Lo scopo di questo lavoro è proporre una metodologia utile per derivare la suscettibilità Stress Corrosion Cracking partendo dall'analisi dei test descritti nello Standard UIAA (ASTM G36 and ASTM B117). L'UIAA propone due standard di resistenza alla corrosione che però non tengono conto della presenza della cricca che ne modifica la resistenza. Cricca che deriva dalla vaiolatura del componente per innumerevoli ragioni [1]. Per rimediare a ciò, si propone di seguire le regole di frattura e quindi valutare il K_{EAC}. Per determinare l'efficacia della metodologia, sono stati preparati campioni in tre diversi materiali (sempre proposti da UIAA come candidati per l'applicazione), in particolare AISI 316L, SAF2205, Titanio Grado 5 e successivamente è stato preparato il test. Il test dopo trenta giorni ha mostrato che i materiali sono ancora buoni per la loro applicazione. Inoltre, la tecnica si dimostra affidabile e consente di ottenere maggiori informazioni sulla velocità di degrado, sui tempi e sui carichi applicati.

Parole chiave: Stress Corrosion Cracking; Ancoraggi da roccia; Acciaio inossidabile Titanio; Tenacità a frattura; Propagazione della cricca.

Contents

1.   Rock anchors for sport climbing

1.1   Sport climbing background

Sport-climbing has become an increasingly popular sport since the '80s, when the first pioneers laid the foundations of this fun activity. Today rock climbing (Figure 1) on limestone cliffs in warm marine environments in particular has grown in popularity because of several factors: availability of leisure time and money, higher mobility, boredom and need of adventure. Significant improvements of safety standards, and intense advertising campaigns made this sport more attractive to a broader public [1].

Figure 1 An example of rock climbing

The increasing number of people approaching climbing, led to an increment of the so-called world climbing destinations (WCD), which are equipped areas (from the Mediterranean coasts of Greece, Italy, Spain, France, Turkey to the far-off beaches of South Asia, e.g. Thailand and Laos) where it is possible to combine the beauties of rustic locations, delicious exotic food, pleasant company, wonderful rocks, interesting routes and the romantic views of the sunset over the sea. On the other hand, with the growth of seaside climbs around the world, there has been an increasing number of accidents related to anchor failures.

1.2   Main climbing technique

There are main techniques to ascend climbing routes; one of the most used is the lead climbing technique. In this technique there is a lead climber attached to the dynamic rope that ascend the route while periodically attaching protections and at the same time a second person, using a belay device, grants the safety of the climber in case of fall (Figure 2). The following of the second climber is typically much less of risk since he is belayed by a taut rope from above [2]. The critical part is always the ascent of the leader.
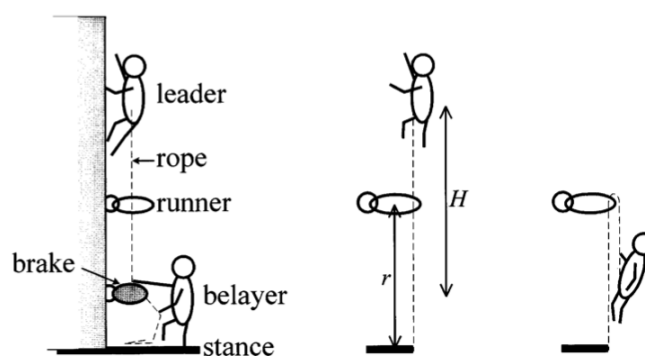
Figure 2 Scheme of lead climbing progression and fall

The protections can be fixed anchors (metal rings already fixed on the rock) or they can be quick protection, consisting in gear that the climber bring with himself. Any fall of the leader will follow basic physical laws imposed by gravity, resulting in a constant acceleration until the rope becomes taut and the fall can be stopped by the belayer using a brake.

1.3   Type of anchors

Basically, two types of climbing anchors (Figure 3) exist to serve as fixed climbing protection apparatus: glue – in bolts and expansion bolts [1].

Figure 3 Picture of an anchor fixed in the rock

1.3.1 Glue – in bolts

They are recognized as the most durable bolts used in rock climbing today. These kinds of bolts (Figure 4) are essentially a piece of high – grade bar stock glued into a drilled hole with construction grade epoxy.

Figure 4 Glue - in bolt

They can vary slightly in shape and composition, but all of these type of bolts have in common a ring on one end for clipping. Having no metal on metal contact or moving parts and largely encased in a waterproof epoxy, they resist corrosion more than any other bolts. On the other hand, these bolts are perhaps the most difficult to be placed. Glue – in bolts are available in 304 and 316 stainless steel, while for particularly corrosive environments they are made of titanium. Most glue – in bolts are placed in a hole drilled slightly larger than the diameter of the bolt itself; this allows the epoxy to encase the bolt, forming in this way a reliable bond with the rock (Figure 5).

Figure 5 Glue - in bolt fixed in the rock

Because of the importance of this bond between the bolt and the rock, cleaning very well the hole is an extremely important phase when using glue – in bolts.

1.3.2 Expansion bolt

Expansion bolts (Figure 6) are the widest installed bolts because of their low cost and easiness of installation, if made by stainless steel they can last several decades also in aggressive environments.

Figure 6 Components of an expansion bolt

They consist of a threated bolt with a single or double conical end wrapped in a clip. A nut and a washer are attached to the threated end. This kind of bolt is installed

being hammered into a properly sized hole and as it is tightened the cone pulls forward causing the clip to grip inside the hole (Figure 7).
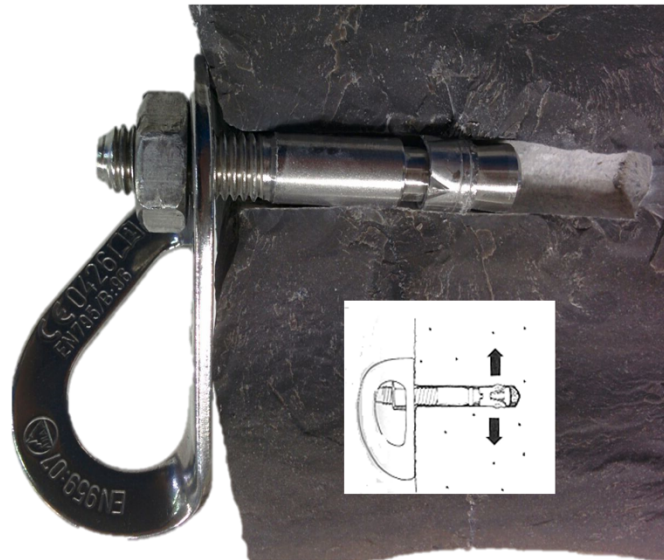

Figure 7 Scheme of an expansion bolt

To place this type of bolt, first a hole need to be drilled in the rock (diameter of the drill equal to the diameter of the bolt); the hole must be perpendicular to the rock and in a flat area; an air pump is required to remove the dust from the hole and finally the bolt can be hammered.

1.4   Failure of rock anchors

Anchors made of stainless steel have been widely used for rock anchoring in marine environments. The presence of corrosive environment, the tightening induced stresses and the susceptibility of the anchor material to stress corrosion cracking are the most critical parameters that may influence the life of the anchor [3]. Failure analysis finding suggest that the failure was caused by stress corrosion cracking. The anchor experienced extensive cracking during its lifetime and eventually broke when an unsuspected climber attempted to hang from it. One of the main causes of the

failure of rock anchors in marine environments is stress corrosion cracking [4] and there are some factors contributing to this problem [6]:

- Concentration of chloride: chloride deposits containing salts with high solubility can be formed;

- Temperature: SCC could starts at 20°C, an higher temperature increases the cracking speed; the temperature of a bolt in the sun can be significantly higher than the ambient temperature;

- Humidity: low relative humidity, between 20% and 70%; RH close to the deliquescence point of the chloride solution poses a significant danger SCC. Localized RH of the anchor can be significantly different from ambient RH, for example exposed to the sun;

- Location: next to the sea; there is no clear limits; winds from the sea with significant salt concentration can travel very far inland;

- Rock type: some rock types can create worse conditions than others, depending on specific circumstances.

Climbing anchors are elements fixed on rocks (Figure 8) and these natural structures show very variable rock, depending on the geographic position. In the most common case where anchors are fixed, the mineral is limestone, in particular tower karst [7].

Figure 8 Anchor fixed in the rock

This type of limestone is presented by the formation of rocky structures with a height between 30 and 300 metres, and with vertical or overhanging walls. It differs from common limestone because of washout of atmospheric agents, which over the years have eroded the structure, causing the formation of rocky complexes full of caves, inlets and stalactites.

This effect is accentuated by the high levels of CO_2 in water present in soils caused by the abundance of microorganisms and vegetables typical of these areas, which lead to soil acidification through the formation of carbonic acid - H_2CO_3. Although the chemical composition of limestone varies considerably not only according to the location, but also to the position on the rock face, some characteristics can reasonable be considered constant. In particular, the presence in the mineral of compounds such as calcium carbonate $CaCO_3$ and magnesium $MgCO_3$. The erosive effect therefore leads to an enrichment of the water in products containing these two elements, which subsequently form solution with gradually higher concentration due to solar irradiation which causes the water to evaporate. These phenomena occurring on the rock can also be cause of the failure of rock anchors as it is shown in Figure 9.

Figure 9 Examples of failure of rock anchors

2.   Stress Corrosion Cracking (SCC) and fracture mechanics

2.1 Stress Corrosion Cracking

Stress corrosion cracking is one of the most important phenomena responsible for the failure of rock anchors as it is shown in Figure 10. The material's failure occurs mainly by the combined effect of corrosion and tensile mechanical stresses, and eventually temperature [8].
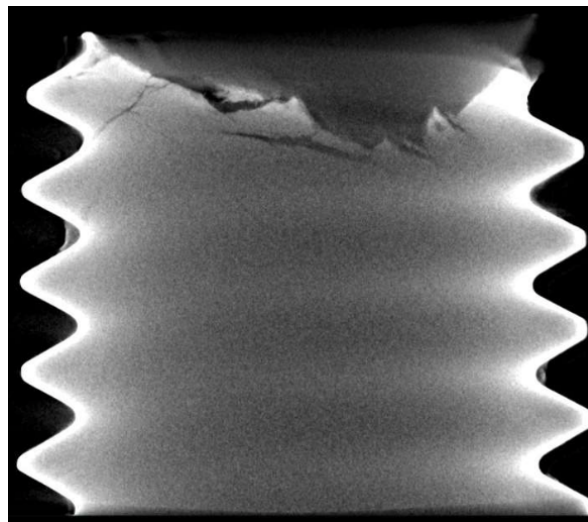

Figure 10 Section of a climbing bolt under
SCC

The overall stress corrosion cracking process can be divided in three main stages (Figure 11):

1. Initiation process: during this stage occurs the development of an occluded cell with its attendant acidification and concentration of anionic species takes place; this development is strongly correlated with pitting or crevice corrosion in stainless steel or other passive materials.

2. Propagation process;

3. Final failure stage;

The SCC phenomenon can be evaluated by different types of experimental tests according to several standards. An important parameter that can be determined testing notched specimens is the K_{ISCC}: the stress intensity factor necessary to propagate a crack by the SCC phenomenon. Figure 11 shows an example of the test stages during the propagation of a crack by this phenomenon. The K_{ISCC} parameter depends on the material composition and the environment. The knowledge of this parameter is important for the structural integrity of components that operate in similar conditions of the tests.
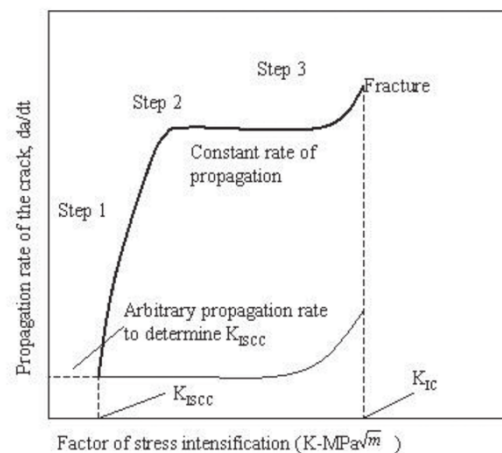

Figure 11 SCC stress intensity factor vs crack propagation rate

2.1.1 Important parameters of SCC

The SCC phenomenon occurs when three factor exist: a susceptible material, an aggressive environment, and tensile stresses (residual or from service). The main features of each of these factors are described below:

- *Tensile stresses*: this is the most important parameter for this type of phenomenon; stresses arise from residual stress due to welding, forming or heat treatment, or from applied loads. Below the macroscopic yield stress, stresses are sufficient to cause SCC, but propagation rates are also influenced by the magnitude of the stress. It is also known that SCC occurs only if the strain rates are within an initial range limited by the upper and the lower bound critical strain rates. The magnitude of stress required for SCC depends on the material microstructure and the environment [8].

- *Environment*: usually they are aqueous solutions; it is generally observed that some specific chemical species can cause SCC, but it also depends on the alloy of the metal considered: a species that can cause SCC in a certain alloy, could be not dangerous for another alloy. Changing in temperature or in the degree of aeration can change a non-corrosive environment into a corrosive one, causing SCC. The solubility of the reaction product in the environment is an important factor in the crack propagation by SCC. In order to propagate, the crack has to be limited along the crack faces; in this way there is the formation of some surface films that can be passive or a layer of precipitated corrosion product [9].

- *Material - alloy chemistry and microstructure*: they're the two other important parameters; alloy composition, concerning impurity and trace elements, and metallurgical conditions as strength levels, composition of phases and grain boundary, affect in a very significant way the SCC behaviour. In fact, by working on the microstructure or on the alloy chemistry, it is possible to have a material which is immune or particularly resistant to SCC [8].

Eventually, the temperature can influence the crack advance and make it grows in faster velocities. The main characteristics of the influence of the temperature are described below:

- *Temperature*: The effect of temperature is certainly one of the parameters to be taken into consideration for the phenomenon of stress corrosion cracking; on the one hand, high temperatures could accelerate the process, while if it were below certain values, the phenomenon could not occur. In this case, at temperatures around 50 °C, which can be reached for example under the midday sun in seaside locations, the steel heats up and the SCC phenomenon is accelerated; this temperature value is critical for the AISI 300 family.

2.2 Fundamentals of fracture mechanics

In the following sub-chapter, some fundamentals about fracture mechanics are described, also including its application in stress corrosion cracking problems.

2.2.1 Linear elastic fracture mechanics

Figure 12 schematically shows an element near the crack tip in an isotropic linear elastic material also with the in–plane stresses on this element [10]. Each stress component is proportional to a single constant K_I; if this constant is known, the entire stress distribution at the crack tip can be computed with the equations described in the Figure 12. This constant is called *Stress intensity factor* and characterizes the stress field at regions near the crack-tip in a linear elastic material [10].

$$\sigma_{xx} = \frac{K_I}{\sqrt{2\pi r}} \cos\left(\frac{\theta}{2}\right)\left[1 - \sin\left(\frac{\theta}{2}\right)\sin\left(\frac{3\theta}{2}\right)\right]$$

$$\sigma_{yy} = \frac{K_I}{\sqrt{2\pi r}} \cos\left(\frac{\theta}{2}\right)\left[1 + \sin\left(\frac{\theta}{2}\right)\sin\left(\frac{3\theta}{2}\right)\right]$$

$$\tau_{xy} = \frac{K_I}{\sqrt{2\pi r}} \cos\left(\frac{\theta}{2}\right)\sin\left(\frac{\theta}{2}\right)\cos\left(\frac{3\theta}{2}\right)$$
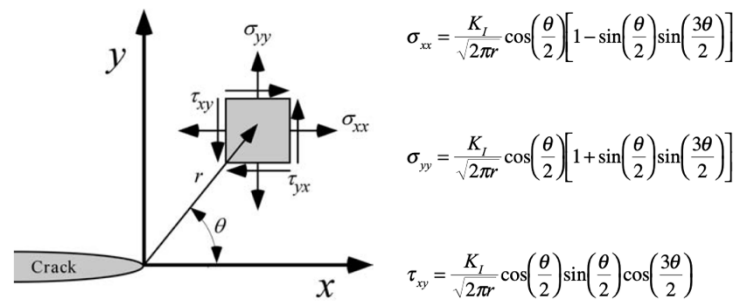
Figure 12 Stresses near the crack tip of an elastic material and their equations (from [10])

The general solution for the stress intensity factor is as follows:

$$K = Y\sigma\sqrt{\pi a} \tag{1}$$

being Y a factor depending on geometry and loading conditions, σ the applied stress and a the crack length. If the assumption that a material containing a crack fails at some critical combination of stress and strain at the crack-tip it is possible to say that fracture occurs at a critical stress intensity factor identified by K_{Ic}. Failure occurs when $K_I = K_{Ic}$. In this situation the first parameter is called the crack-driving force for fracture, while the second is the material plain-strain fracture toughness. The ASTM E399 standard [13] describes the procedure for the fracture toughness determination for materials that present a linear-elastic behavior. Figure 13 presents some typical linear elastic behaviors, from which the fracture toughness can be determined. Those Load vs. CMOD plots are recorded during the loading of standardized specimens. Before the fracture tests, a fatigue pre-cracking procedure need to be performed to replicate a sharp defect that can be originated during the service life of the

component. After this, the specimen is positioned in the testing machine and it is

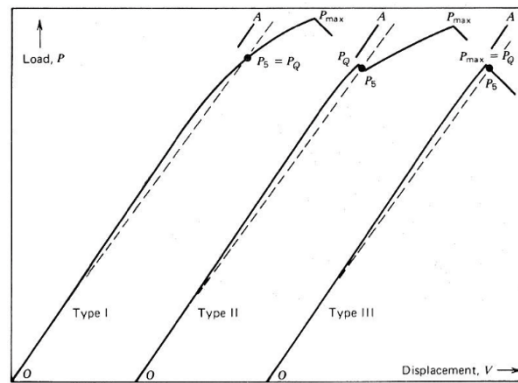loaded, according to standards.

Figure 13 Load vs crack mouth opening displacement plot.

From the plots shown in the figure above and after some specific verification of the

material behavior, P_Q values are determined and used to calculate the K_Q, an interim
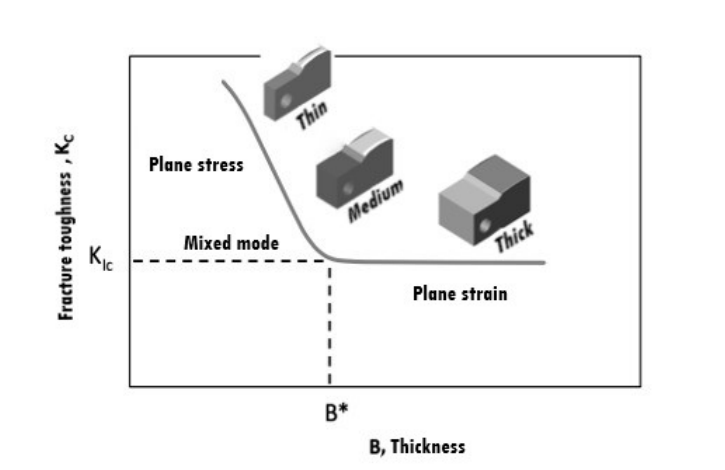
plane-strain fracture toughness value.

Figure 14 Relationship between K and B.

As described in Figure 14, K_Q depends on the thickness of the specimen. If a critical specimen thickness B is exceeded, K_Q remains constant, assuming the lowest possible fracture toughness value for the material (K_{Ic}). This condition, corresponding to fully plain strain condition, is the most conservative. Such condition is verified when the plastic radius ahead of the crack tip is much smaller than B and W-a (uncracked ligament). This real plain strain condition is present when:

$$B, (W - a) \geq 2{,}5 \cdot \left(\frac{K_Q}{\sigma_{ys}}\right)^2 . \tag{2}$$

2.2.2 Fracture mechanics in stress corrosion cracking

Stress corrosion cracking (SCC) is considered as a problem of long standing. It manifests itself as a *delayed failure* [11] mode: a failure which occurs after some period of structural component under statically applied loads, at stresses well below the yield strength of the material. The traditional measure used for stress corrosion cracking susceptibility is given in terms of the time necessary to produce failure at different stress levels, obtained from testing smooth or notched specimens. Figure 15shows an example of a notched specimen geometry, in this case the SE(B) geometry.
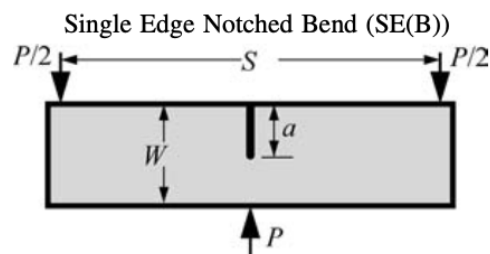

Figure 15 Example of notched specimen.

The failure time incorporates both the time required for crack initiation and a period of a sub-critical crack propagation, and to separate the effect of the environment on each of these stages cannot be ascertained. To test this phenomenon, much of the attention was devoted to understanding the electrochemical reactions responsible for metal dissolution, crack nucleation and time–to–failure under a constantly applied load or strain in corrosive environments. From the design and engineering perspective using the fracture mechanics parameters and concepts, it is important to focus on the determination of a threshold stress intensity factor that would provide some safety conditions over the service-life of the component or structure. In particular, for the SCC phenomenon, the K_{EAC} and crack growth rate (*da/dt vs. K*) curves are important fracture properties during this phenomenon. An example of crack growth rate curve can be seen in Figure 16.
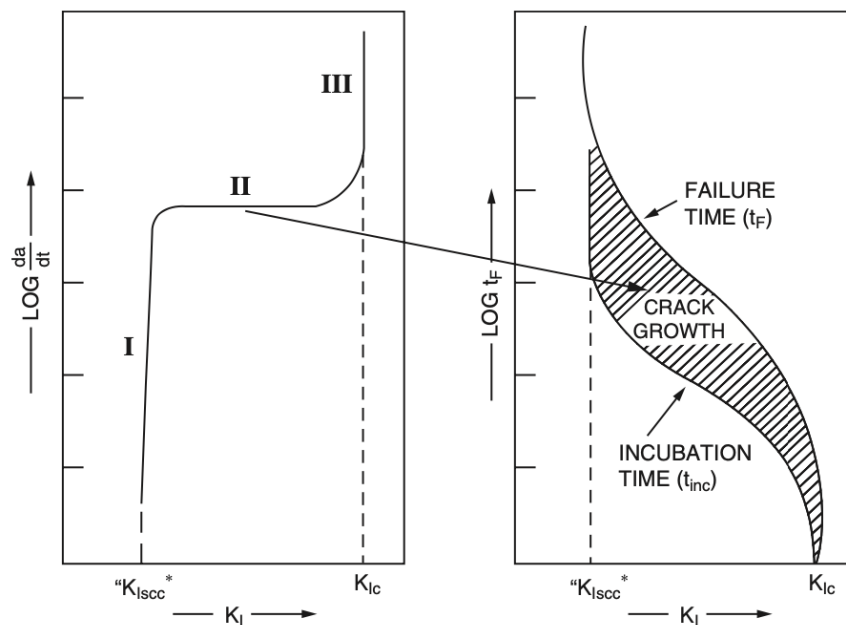

Figure 16 Typical SCC response (from [11]) in terms of steady - state crack growth (left) and time (right).

3.   Materials and methods

The aim of this work is the determination of the K_{ISCC} in a distilled water solution with 3.5% of NaCl. Three different alloys were studied:

- AISI 316L, stretched: marine series of anchors produced by Raumer. Limited C and stress relieving serve to improve corrosion resistance. Less carbon available more Cr to make the passive film and the distension removes residual stress.
- SAF2205 (Duplex);
- Titanium – grade 5.

The second and third alloys were chosen following the UIAA communication of 2015. The nominal chemical composition of these three alloys are reported in Table 1, 2 and 3. Basically, those materials are two stainless steels (austenitic grade AISI 316 and duplex SAF2205) and Titanium alloy grade 5.

Table 1 Nominal chemical composition of 316L

Steel grade			Typical chemical composition				
UNS	ASTM	EN	% Cr	% Ni	% Mo	% N	% Others
S31600	316L	1.4401	17,2	10,2	2,1	-	-

Table 2 Nominal chemical composition of 2205

Steel grade			Typical chemical composition				
UNS	SAF	EN	% C max	% Cr	% Ni	% Mo	% N
S31803	2205	X3NiMo2205	0,03	22	5	3	0,16

Table 3 Nominal chemical composition of Titanium Grade 5

Steel grade	Typical chemical composition						
Ti6Al4V	% N	% C	% H	% Fe	% O	% Al	% Others
Grade 5	0,05	0,10	0,0125	0,30	0,20	6,00	4V

3.1 Materials microstructure analysis

In this section, the microstructural analysis will be described as well as the hardness and tensile tests. The procedure is given by ASM Metal Handbook Volume 9 "Metallography and microstructure" [17].

3.1.1 Cutting and cleaning of samples

As a first step, samples were taken. The collection of samples is carried out by cutting the component using a miter saw, in order not to thermically alterate the structure. One sample for each material was cut. The dimension of the sample must be such as to allow the study on a representative surface of the sample and to allow easily handling the sample for subsequent operations [12]. The next step was the incorporation of the samples in an epoxydic resin in order to obtain pieces that was easier to handle. Then, in order to carry out a proper metallographic observation,

some cleaning operations must be done; firstly, in order to obtain clean, smooth, free from scratches and deformations surfaces, the interested faces of the samples was abraded using a mechanical polisher with an highly abrasive paper changed periodically with smaller grit size (from P120 to P2500). To remove the last scratches a velvet polishing pads with 1μm diamond paste was used.

3.1.2 Etching

Once the samples have been polished, they are ready for the etching, in order to reveal the microstructure in terms of grain boundaries and second phases. Etching is performed by immersing the sample in a particular reactive solution for the necessary time; then the sample will be properly cleaned and dried. If there is the situation od electrochemical attack, solutions used are different and also low currents and voltage are needed.

For each material a different kind of etching was performed:

- **AISI 316L**
    - Type of etching: Electrochemical etching with Oxalic acid (Figure 17);
    - Composition: 10g of Oxalic Acid in 100 ml of H_2O;
    - Parameters of the machine: 6V.

Figure 17 Electrochemical etching
with oxalic acid

- **SAF 2205**

  - Type of etching: Beraha (Figure 18)

  - Composition: 20 ml of HCl, 100 ml of H_2O, 0,1g of $K_2S_2O_5$, 2,4g of $(NH_4)HF_2$;
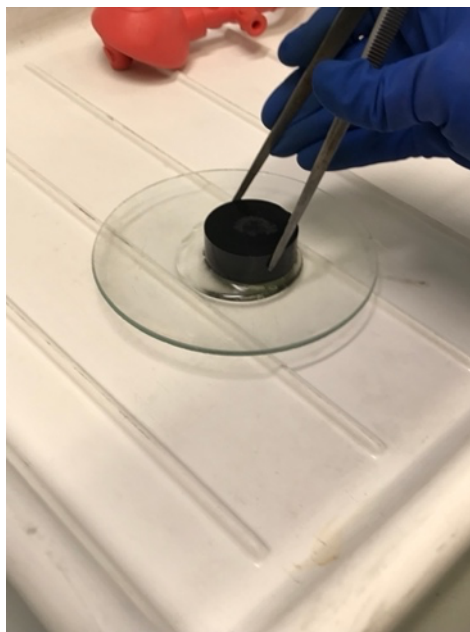
  - Time of etching: 45 seconds.

Figure 18 Beraha etching

- **Titanium Grade 5**

  - Type of etching: Kroll;

  - Solutions: 58 ml of of H_2, 6 ml of HNO_3 and 2 ml of HF;

  - Time of etching: 10/15 seconds.

3.1.3 Hardness test

Two different tests were performed in order to determine the hardness of the three materials: Rockwell test (HRC) and Vickers test (HV). For HV test the loads applied

were of 300g and 500g for 15 seconds. The test followed the standard ASTM E 18 - 07 for the Rockwell and ASTM E92 – 17 for the Vickers.

3.1.4 Tensile test

Tensile test is needed to know the mechanical properties in term of yielding, maximum stress, and elongation of the materials. These tests were done on the three materials after machining to obtain specimens according to the standard (ISO 6892). The standard also provided all the test characteristics. One specimen was obtained for each material and then was tested. The test speed was 2 mm/min. In Figure 19 it is reported the geometry of the specimen used during the test.
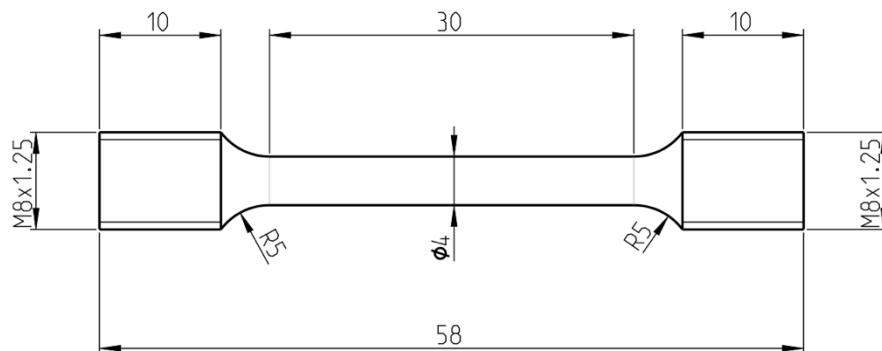

Figure 19 Specimen geometry for tensile test

4. Fracture test assisted by corrosion

As already mentioned, the UIAA 123 (2021) is the referring standard for mountaineering equipment; this standard proposes two different tests for rock anchors ASTM G36 and ASTM B117:

- According to ASTM G36 – 94: This practice describes a procedure for conducting stress-corrosion cracking tests in a boiling magnesium chloride solution. Although this test may be performed using various concentrations of magnesium chloride, this procedure covers a test solution held at a constant boiling temperature of 155.0 6 1.0°C (311.0 6 1.8°F). The boiling magnesium chloride test is applicable to wrought, cast, and welded stainless steels and related alloys. It is a method for detecting the effects of composition, heat treatment, surface finish, microstructure, and stress on the susceptibility of these materials to chloride stress corrosion cracking. The duration of this test indicated in UIAA 123 is about one week;

- According to ASTM B117: This practice covers the apparatus, procedure, and conditions required to create and maintain the salt spray (fog) test environment. The apparatus required for salt spray (fog) exposure consists of a fog chamber, a salt solution reservoir, a supply of suitably conditioned compressed air, one or more atomizing nozzles, specimen supports, provision for heating the chamber, and necessary means of control. The duration of this test indicated in UIAA 123 is about four weeks.

The first experimental procedure described considers the resistance to pitting which will certainly be high for the proposed materials, due to the presence of Mo for AISI 316L and SAF2205, and the non-susceptibility for the Titanium Grade 5. This test is

based only on the presence of sprays and as described in several studies [1], the condition for having pitting from which to start the cracks are many and all almost independent of the presence of chlorine. The other procedure, on the other hand, distorts the conditions with a corrosion that is too aggressive (but which explains the reason for only one week of testing), however not taking into account the presence of notch that derives from the pit (generated as mentioned by different conditions) and not thus offers an idea of the applied loads; with the proposed test instead, it is possible to record these loads and relate them to the properties of the materials. At this point, this work wants to propose a methodology that also takes into consideration the resistance of the materials: through the determination of K_{ISCC} taking into consideration the corrosive environment, the presence of the notch (recreating the pitting condition) and through controlled loading conditions.

4.1 Specimen type and geometry

In this section, the specimens' geometry and the different procedures carried out to prepare the specimens for the tests are described. The fatigue pre–cracking procedure applied to each specimen, the fracture toughness determination in air at room temperature, and all the equipment preparation for the determination of the K_{ISCC} are explained. Both tests, fracture toughness tests in air and the K_{ISCC} tests, were performed using single edge notched bend specimens – SE(B) - according to ASTM E1820 and ASTM E399 standards. This standard bend fatigue pre-cracked specimen is loaded using a three point–bending device with a support span (*S*) equal to four times the width, *W*. Figure 20 shows a schematic representation of the SE(B) specimen).
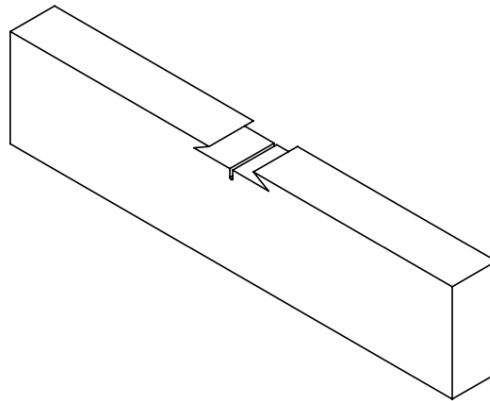
Figure 20 SE(B) specimen geometry.

Figure 21 shows the technical drawing for the SE(B) specimens of AISI 316L and SAF2205. Both materials were tested with specimens of the same dimensions.
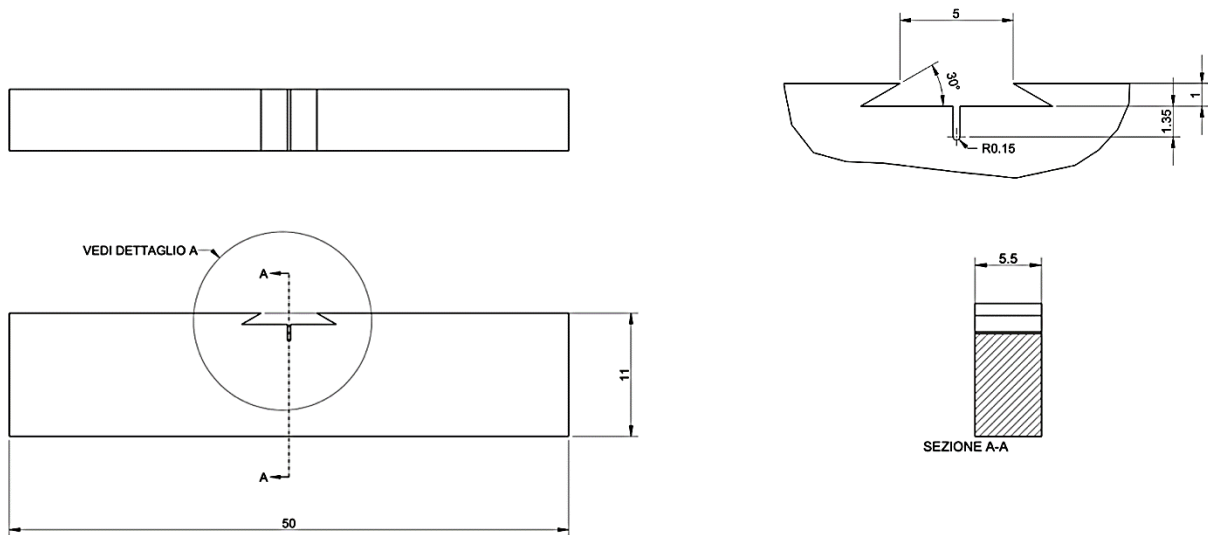

Figure 21 AISI 316L specimen geometry (dimensions in mm).

In Figure 22, is reported the technical drawing of the Titanium Grade 5 specimen with its proper geometry and nominal dimensions.
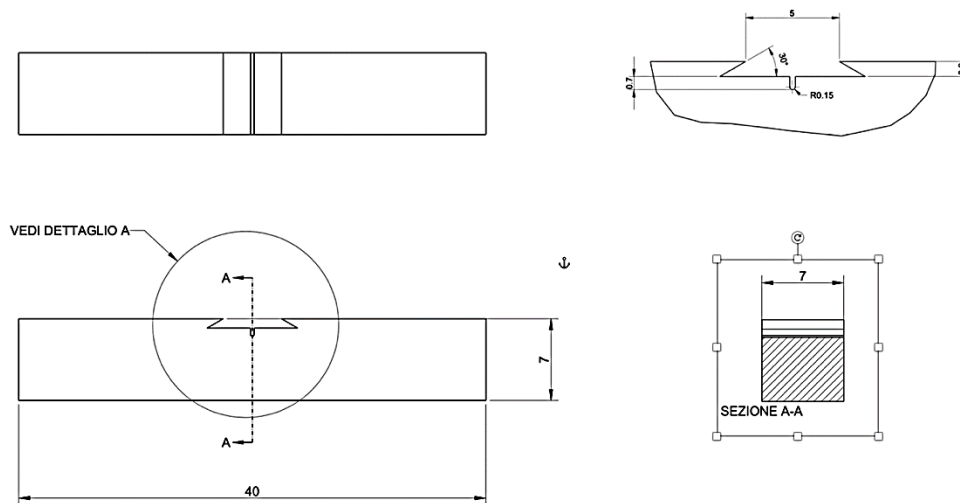

Figure 22 Titanium specimen geometry (dimensions in mm).

Samples were taken from the center of cold drawn bars. This is because this type of semi-finished products (or laminates) are mainly used to make the anchors and which in any case have a microstructure similar to that of the anchors.

4.2 Fatigue pre – cracking preparation

The fatigue pre-cracking procedure was performed according to the ASTM E1820-20 standard, using servohydraulic testing machine or electrodynamic machines. The procedure was performed with stress ratio of 0.1, in air at room temperature. Figure Figure 23 presents a schematic representation of the fatigue pre-crack at the notch-tip and a plot of the cyclic loads.
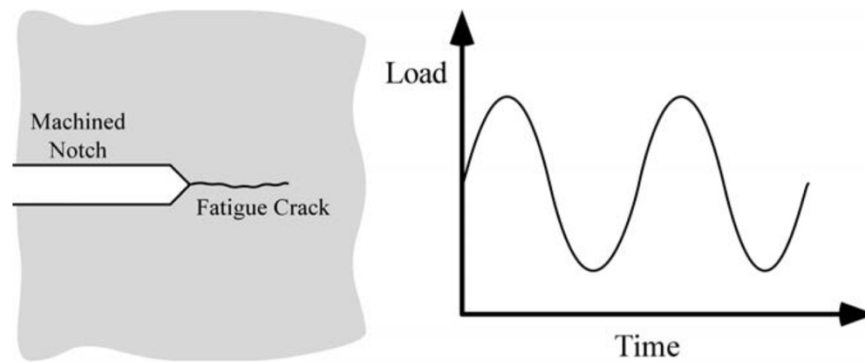
Figure 23 Fatigue pre - cracking scheme (from [10])

At the beginning of the pre-cracking step, a maximum force needs to be calculated for each material. The force P_m is calculated as follows:

$$P_m = \frac{0.5 B b_0^2 \sigma_y}{S} \qquad (9)$$

where σ_Y corresponds to the mean value between σ_{YS} and σ_{UTS} of each material. The value of the force evaluated depends on material properties and specimens' geometry, and in this way it was possible to evaluate the limiting value used with the 3kN machine (Figure 24) in order to pre-crack the specimens.
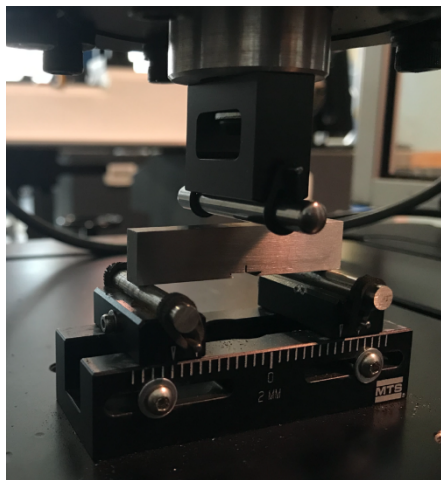

Figure 24 AISI 316L specimen during pre - cracking procedure with 3kN machine

In Table 4 the limiting value of the force are summarized.

<div align="center">Table 4 Limiting value of the force for pre - cracking</div>

Material	AISI 316L	SAF 2205	Ti6Al4V
P_m limit [N]	1806,3	2709,4	2410,0

Through a visual inspection during and after the pre-cracking phase, the length of the crack reached was approximately of 1mm, obtaining in this way a characteristic length a_f useful for the calculation of P_m force; the values obtained are the following (Table 5):

<div align="center">Table 5 Length of the crack before and after pre–cracking procedure.</div>

Material	AISI 316L	SAF 2205	Ti6Al4V
a_i [mm]	2,5	2,5	1,5
Crack length [mm]	1	1	1
a_f [mm]	3,5	3,5	2,5

4.3 Fracture toughness test in air at room temperature

The fracture toughness tests in air at room temperature were performed according to ASTM E1820-18 standard. As described previously, the tests were made using the SE(B) specimen geometry in a MTS Landmark servohydraulic testing machine instrumented with a ± 25 kN load cell. It is important to notice that due to the specimens' dimensions, a fracture extensometer was not used to measure the crack-

mouth opening displacement (CMOD). Instead of it, only the Load (*P*) and the load-line displacement (LLD, or v) were recorded. Figure 26 shows an example of a *P* vs. LLD record. In this figure, it is also shown some useful parameters for the fracture toughness assessment of a material that presented an elastic-plastic behavior during the fracture toughness test.
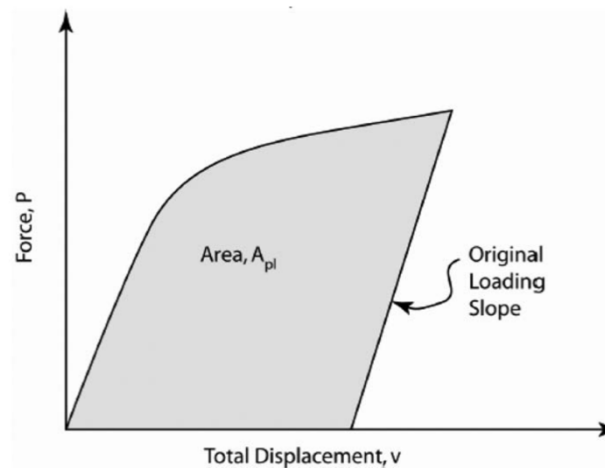

Figure 26 Definition of the area for J
calculation using the basic method

As it will be show, the SE(B) specimens of the three materials presented an elastic-plastic behavior and the evaluations were performed as follows. The *J*-integral parameter was calculated as follow:

$$J = J_{el} + J_{pl} \tag{3}$$

where J_{el} is the elastic component of *J* and J_{pl} is the plastic component. At each instaneous pair of *P* and *v*, on the *P* vs. LLD (*v*) record, J_{el} is calculated as follows:

$$J_{el} = \frac{K^2 (1 - v^2)}{E} \tag{4}$$

Where *K*, for the SE(B) geometry at force *P(i)*, is calculated following the equation below:

$$K_{(i)} = \left[\frac{P_i S}{(BB_N)^{1/2} W^{3/2}} \right] f\left(\frac{a_i}{W} \right)$$

(5)

Where:

$$f\left(\frac{a_i}{W} \right) = \frac{3\left(\frac{a_i}{W} \right)^{1/2} \left[1.99 - \left(\frac{a_i}{W} \right)\left(1 - \frac{a_i}{W} \right)\left(2.15 - 3.93\left(\frac{a_i}{W} \right) + 2.7\left(\frac{a_i}{W} \right)^2 \right) \right]}{2\left(1 + 2\frac{a_i}{W} \right)\left(1 - \frac{a_i}{W} \right)^{3/2}}.$$

(6)

On the other hand, the calculus of the plastic component of the *J*-integral is calculated according to:

$$J_{pl} = \frac{\eta_{pl} A_{pl}}{B_n b_0}$$

(7)

where: A_{pl} = area under force versus displacement record as shown in **Error! Reference source not found.**; η_{pl} = 1.9 using load – line displacement; B_N = net specimen thickness; $b_0 = W - a_0$.
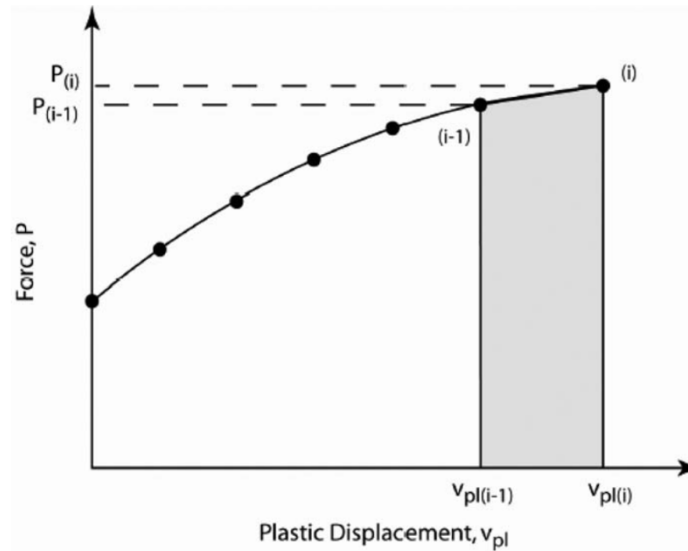

Figure 27 Force versus plastic displacement

The plastic area (A$_{pl}$) is calculated using the following equation:

$$A_{pl(i)} = A_{pl(i-1)} + \left[P_{(i)} + P_{(i-1)}\right]\left[V_{pl(i)} - V_{pl(i-1)}\right]/2 \tag{8}$$

where: $v_{pl(i)}$ = plastic part of the load – line or crack mouth opening displacement = $v_{(i)} - \left(P_{(i)}C_{(i)}\right)$; $C_{(i)}$ = experimental compliance, $(\Delta v/\Delta P)_{(i)}$, corresponding to the current crack size, a_i.

4.4 Equipment preparation for the K_{ISCC} tests

The K_{ISCC} tests were performed using constant displacement technique. Basically, the fatigue pre-cracked SE(B) specimens were loaded by a three-point bending device specially developed for this application. In each device, the load is applied by a screw with a small and hard sphere in the bottom. In this study, cylindrical strain gauges were installed inside the screws to monitor the crack growth during the tests. Before the tests, each screw was calibrated by a universal testing machine. Using the calibrated curves, the deformation measured can be correlated to a load value. **Error! Reference source not found.** shows one of the structural frames with a specimen in position and the instrumented screw. As can be seen in the figure, the frames were covered with an anti–rust spray.
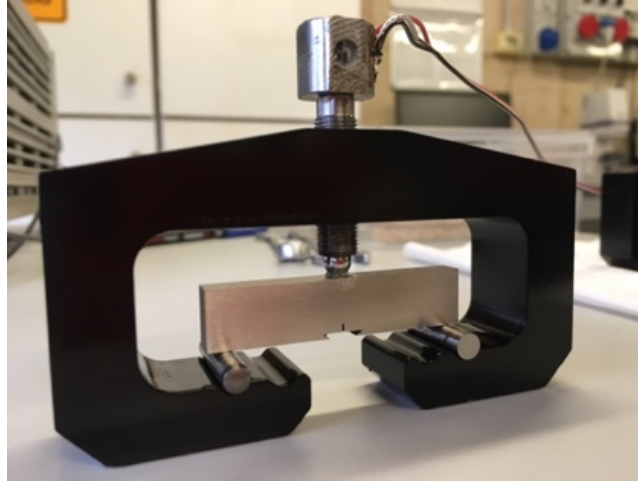
Figure 14 Specimen placed inside a frame with its screw.

After loading the specimens, each frame was put into the 3.5% wt NaCl solution, used to simulate sea water. The deformation of the strain gauges was measured and recorded through an electric control unit.

4.4.1 Strain gauge installation

As described previously, strain gauges were installed in each screw (Figure 29) to measure its deformation during the test. The application was made by technical operators using a particular glue to fix the strain gauges inside small holes. After performing the holes, the fixing glue passed through a curing process performed in two stages:

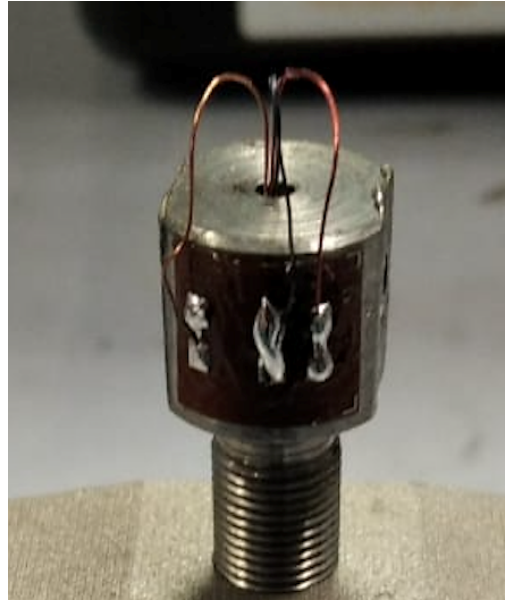   i.   Three hours at 60° C

   ii.   Four hours at 100° C

Figure 15 Particular of a screw with its
strain gauge fixed

4.5 Screws calibration

Before the tests, all screws were calibrated in order to have a proper relation between deformation and applied load. The first necessary step was the welding of the cables on the screw (Figure 30), in order to connect the control unit to each screw.
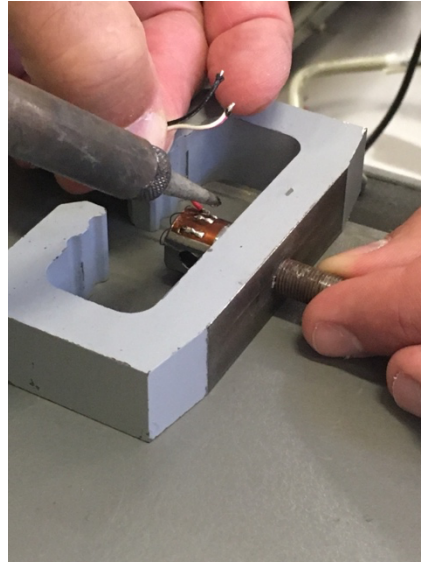
Figure 30 Welding of the cables on the
screw

After welding the cables, each screw was placed on the frame in the opposite orientation respect to the K_{ISCC} test configuration (**Error! Reference source not found.**). Before starting the calibration, the parameters of the machine have been set, in particular:

- 10 V corresponding to 15 kN;
- 20 acquisitions for each loading step applied;
- The loading step selected were 0, 1, 3, 5, 7, 9 kN.

In Table 6 there are summarized the loading step applied converted in Volt to be read from the machine.

Table 6 Conversion from kN to Volt.

V	0,00	0,67	2,00	3,33	4,67	6,00
kN	0	1	3	5	7	9

Once the parameters of the machine have been set, the frame with the screw was placed between the two compression plates, as it is possible to see in Figure 31, and then the calibration procedure started.
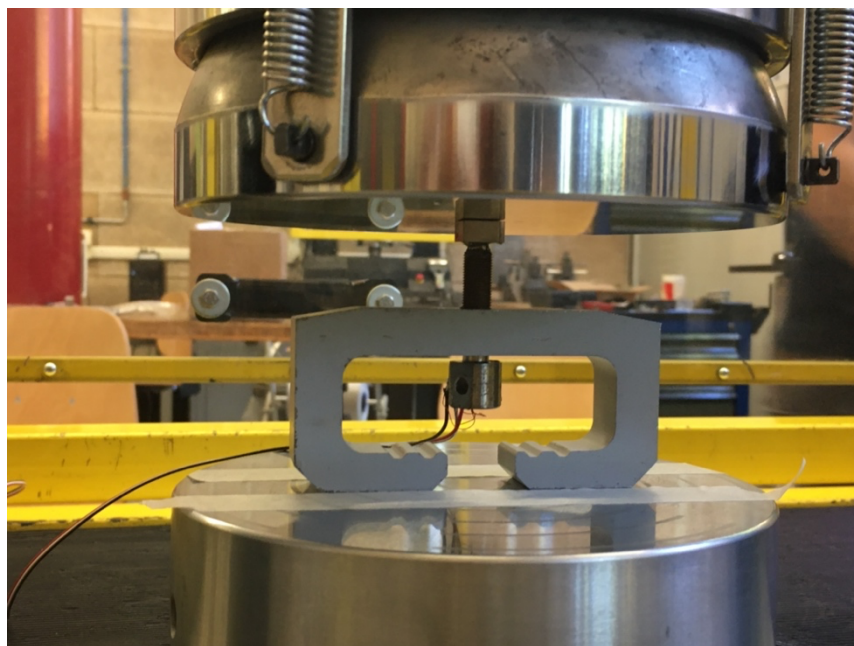

Figure 31 Frame and screw placed between the two compression plates

The purpose of this calibration test is to obtain a linear Strain *vs.* Load plot for each screw.

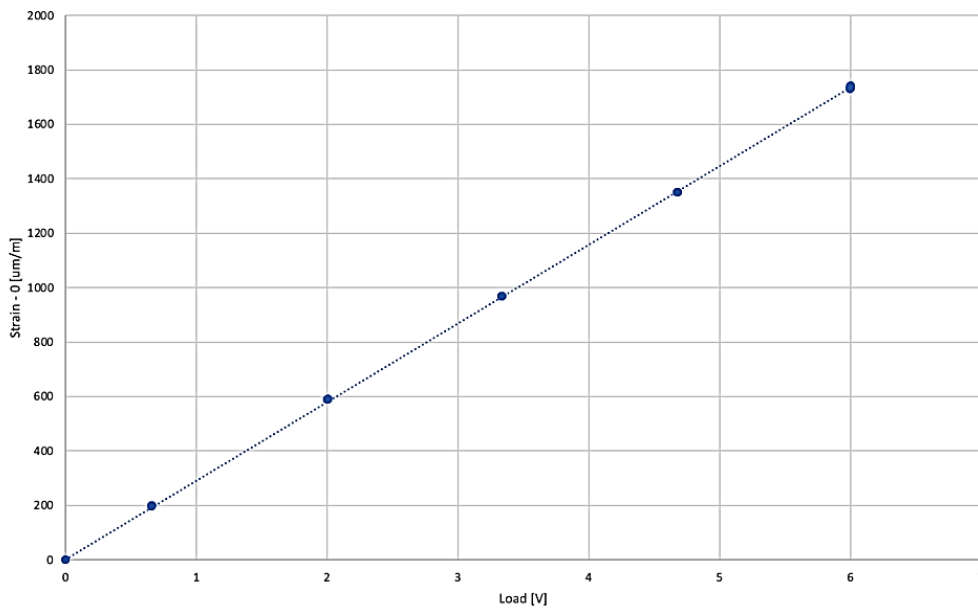In Figure 32 the Strain vs Load plot for the *Screw − 0* is reported:

Figure 32 Strain vs Load plot for Screw - 0

And the respective equation obtained is:

$$y = 289x + 2.96. \tag{10}$$

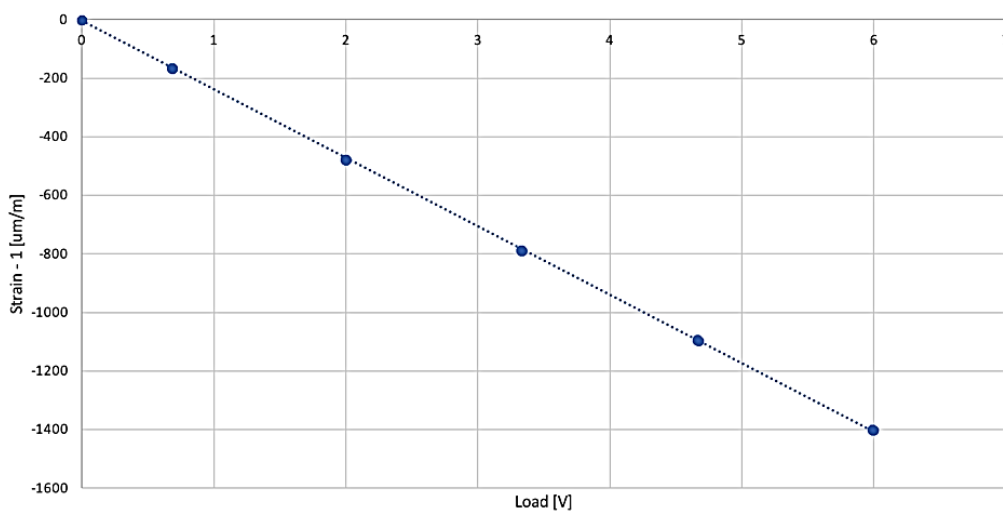In Figure 33 the Strain vs Load plot for the *Screw − 1* is reported:

Figure 33 Strain vs Load plot for Screw − 1.

And the respective equation obtained is:

$$y = -234.27x - 2.50. \tag{11}$$

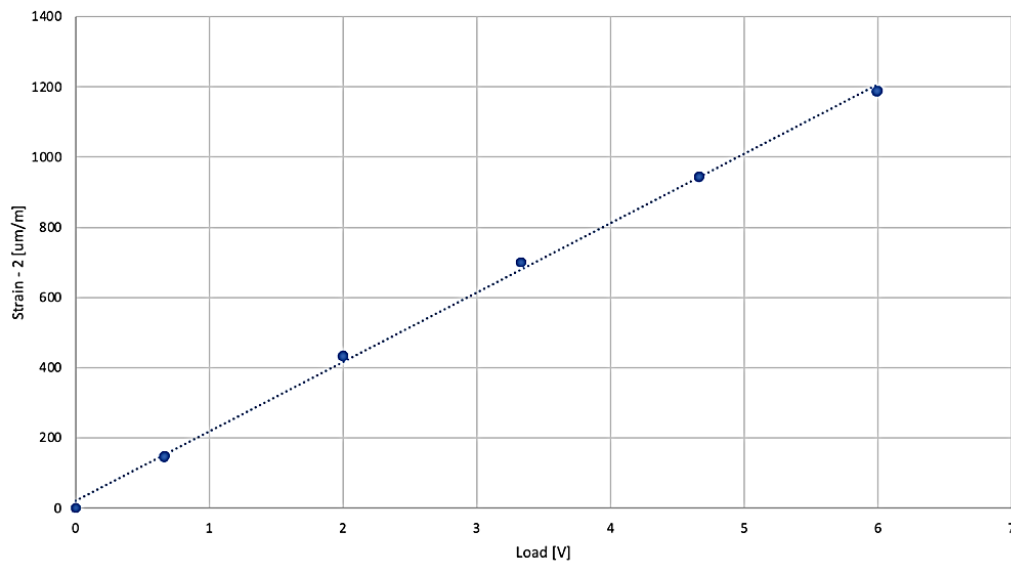In Figure 34 the Strain vs Load plot for the *Screw – 2* is reported:

Figure 34 Strain vs Load plot for Screw – 2.

And the respective equation obtained is:

$$y = 197.95x + 19.79 \tag{12}$$

In Figure 35 the Strain vs Load plot for the *Screw – 3* is reported:
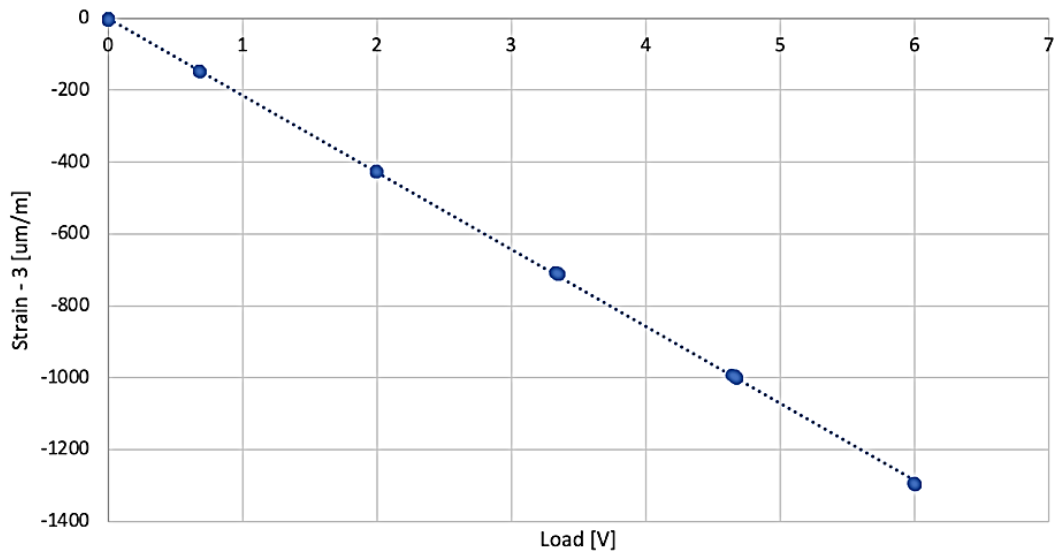
Figure 35 Strain vs Load plot for Screw − 3.

And the respective equation obtained is:

$$y = -214.42 + 0.12 \tag{13}$$

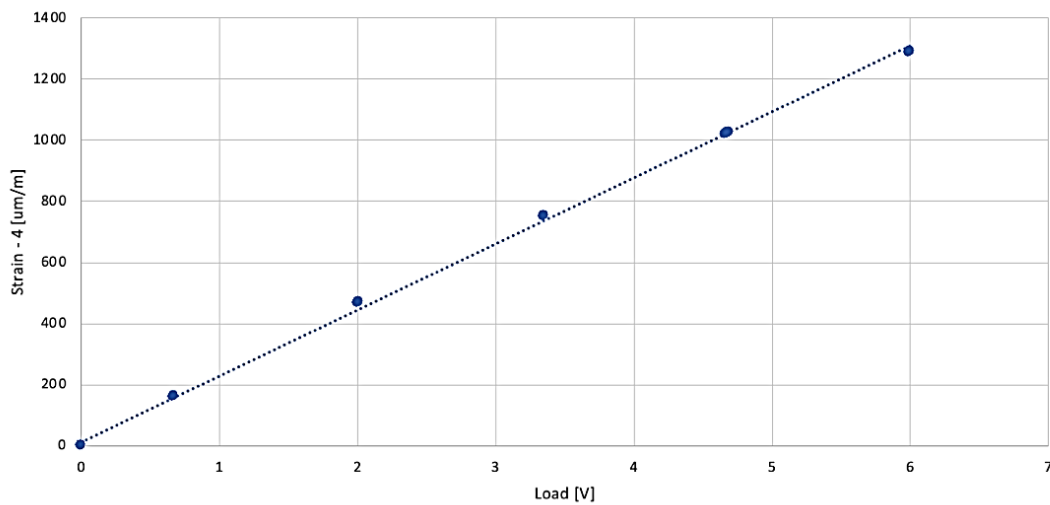In Figure 36 the Strain vs Load plot for the *Screw − 4* is reported:

Figure 36 Strain vs Load plot for Screw − 4.

And the respective equation obtained is:

$$y = 215.92x + 12.79. \tag{14}$$

In this way, selecting a desired K value, there is a correspondent value of Load (in kN) that can be converted in a deformation value. Thus, this value of deformation is applied in the specimen turning the screw.

4.6 Experimental test description

In this section the K_{ISCC} experimental test is described. Different steps during the procedure are required to prepare all the equipment and start the experimental evaluation. A polypropylene box (26x26x15 cm) resistant to temperatures varying from + 5° to + 90° was used. The box is taller to cover all the specimens and the frames until a certain level. In this round of the experimental planning, five fatigue pre–cracked SE(B) specimens were used (one made of AISI 316L, two of SAF 2205 and two of Titanium Grade 5). Consequently, five frame and five screws were prepared as can be seen in Figure 37.
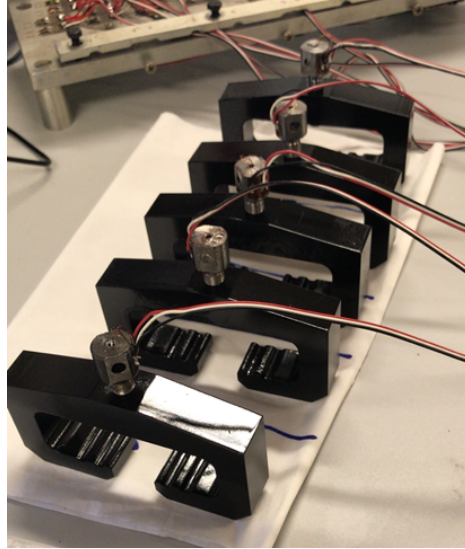
Figure 37 Frames and screws before the test

For the load application, there is a limit for the K application. It means that if this limit is passed, the crack-tip condition will be out of the validity for the K. According to ASTM E1681, this limit of K relative to the limit for the linear-elastic behavior of each specimen is calculated following the equation below:

$$b_0 = \frac{4}{\pi} \left(\frac{K}{\sigma_{ys}} \right)^2,$$
(15)

and deriving the different values of K from (9) using:

$$K = \sigma_{ys} \sqrt{\frac{\pi b_0}{4}}.$$
(16)

As can be seen, to evaluate K for each specimen, the variables used are:

- $b_0 = W - a$ measured for each specimen;
- σ_{ys} evaluated for each specimen in the tensile test described in section 3.1.4.

In Table 7 there are summarized the values of b_0 used to derive K for each specimen:

Table 7 Values of b_0 used for evaluating K.

Specimen	AISI 316L	SAF 2205	SAF 2205	Ti6Al4V	Ti6Al4V
b_0 [mm]	7,17	7,14	7,19	4,13	4,27

In this study, lower values of K were applied in each specimen, in order to have a more conservative approach and to be sure, at the beginning, that specimens were inside the linear-elastic range. For the SE(B) geometry, the K was calculated according to the ASTM E1820 standard using the following equation:

$$K = \left[\frac{PS}{(BB_N)^{1/2}W^{3/2}}\right]f\left(\frac{a}{W}\right). \tag{17}$$

Using the equation above, it is possible to solve in terms of the load, as follows:

$$P = \frac{K(BB_N)^{1/2}W^{3/2}}{S f\left(\frac{a}{W}\right)}. \tag{18}$$

In Table 8 there are summarized the geometric parameters used to derive P.

Table 8 10 Geometrical parameters of the specimens used to derive P.

Specimen	AISI 316L	SAF 2205	SAF 2205	Ti6Al4V	Ti6Al4V
$B\ [mm]$	5.47	5.48	5.47	6.96	6.95
$B_N\ [mm]$	5.47	5.48	5.47	6.96	6.95
$W\ [mm]$	10.96	10.95	10.93	6.95	6.95
$S\ [mm]$	43.48	43.80	43.72	27.80	27.80
$f\left(\dfrac{a}{W}\right)$	1.71	1.72	1.70	2.02	1.91

Once the loads have been calculated, they must be converted from kN to V., according to the conversion relationship used during the calibration phase described in section 4.5 as follows:

$$10\ V = 15\ kN. \tag{19}$$

At this point, having all the loads converted in Volts, it is possible to apply the desired deformation ($\mu\varepsilon$) in each specimen. Then, each specimen was placed in its frame (Figure 38) and the relative load was applied by tightening each screw until reaching the corresponding deformation value.
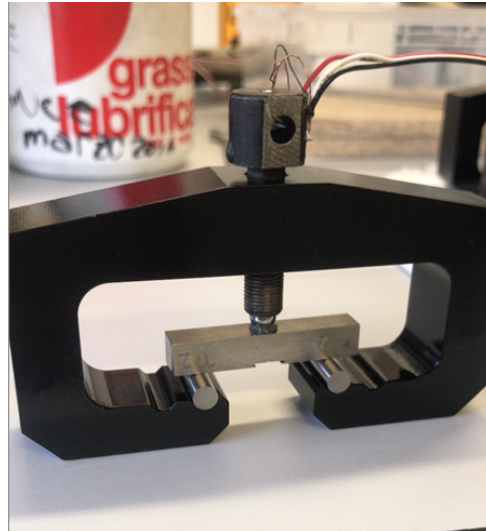
Figure 38 Titanium specimen placed in its frame before tightening

Figure 39 shows an example of the records acquired by the control unit.
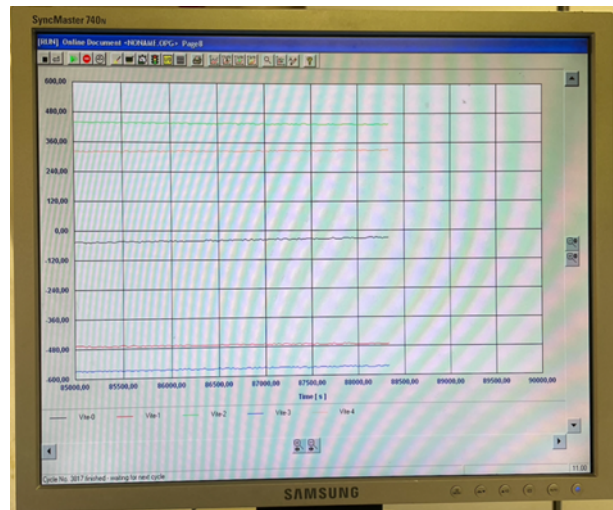

Figure 39 - Control unit

At this point each frame was placed inside the box with the solution and the test was started (Figure 40).

Figure 40 Box with the solution and the frame

To control the temperature during the tests, a thermocouple was connected to the control unit, as can be seen in Figure 41.

Figure 41 – Temperature control

5. Results and discussion

In this chapter the results of all the tests described in Chapter 3 and 4 will be presented and discussed. This section will start presenting the results of the materials microstructures, then the results of the hardness tests, tensile tests, fracture toughness tests in air and the K_{ISCC} tests will be presented.

5.1 Microstructure's results

After etching the samples, some images at the optical microscope have been collected for each material. Figure 42 shows the microstructure of the cross section of the bar in AISI316L. The microstructure is completely austenitic, the grain is coarse and no deformation twins or martensite (ε') resulting from cold processing are evident. This is consistent with the thermomechanical history undergone by the co-imposing. The black spots that can be seen are due to chemical attack and manganese sulphides which increase the machinability of this material with machine tools.
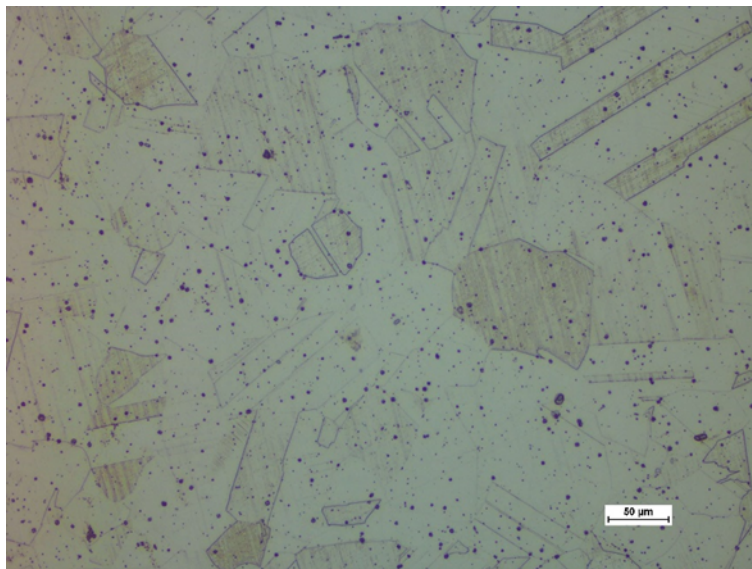

Figure 42 Microstructure of AIS316L by optical microscope

Figure 43 shows the microstructure of the cross-section of the SAF 2205 bar. The microstructure is biphasic composed of ferrite and austenitic in a ratio of 1 to 1. No embrittlement phases are noted (such as σ, τ) which reduce corrosion resistance and toughness of the material. The microstructure is consistent with the thermomechanical history undergone by the component.

Figure 43 Microstructure of SAF2205 by optical microscope
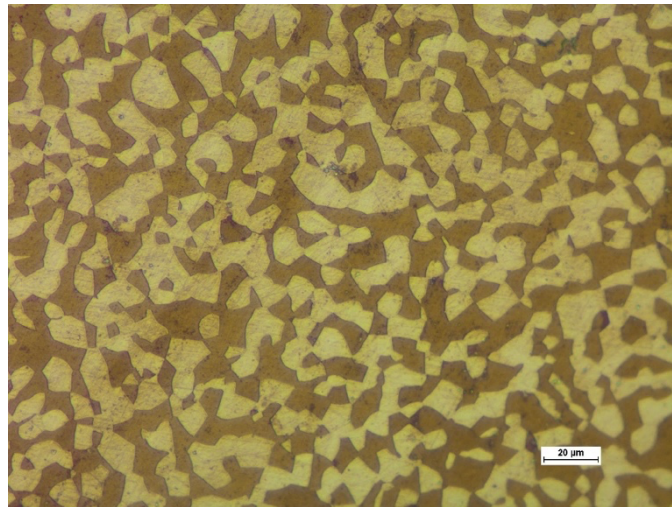
Figure 44 shows the microstructure of the cross section of the Ti6Al4V bar. The microstructure is biphasic composed of grains of primary α (white) and of β transformed in an intergranular position (dark). The microstructure is consistent with the thermomechanical history undergone by the component.
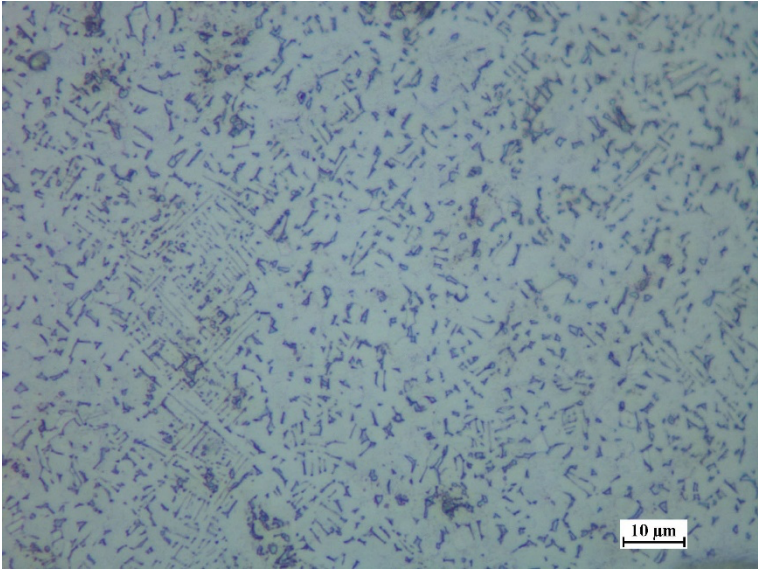
Figure 44 Microstructure of Ti grade 5 by optical microscope

5.2 Hardness test results

HV micro indentation test and HRC macro hardness test were performed on the three materials. In Table 9, the results of the tests are summarized.

Table 9 Results of the hardness tests

Test performed	AISI316L	SAF2205	Ti6Al4V
HV 500g	165.5 ± 10.3	228.0 ± 2.5	279.6 ± 8.7
HV 300g	168.8 ± 15.3	229.8 ± 17.1	308.2 ± 2.9
HRC	28.3 ± 1.2	30.0 ± 0.0	30.7 ± 0.6

The results in the table show the fact that AISI 316L has the lowest hardness value since it has been stretched. SAF2205 shows intermediate hardness values because of its finer structure and biphasic nature; Titanium grade 5 has the finest structure, and the presence of β transformed increases its hardness. For what concern HRC test, being macroscopic, all the mentioned information has been lost and so the hardness values are similar.

5.3 Tensile test results

Three specimens, one for each material was used to perform the tensile test. in Figure 45 there are reported the real stress versus the real strain graphs of the tensile test performed for each material. In its turn,
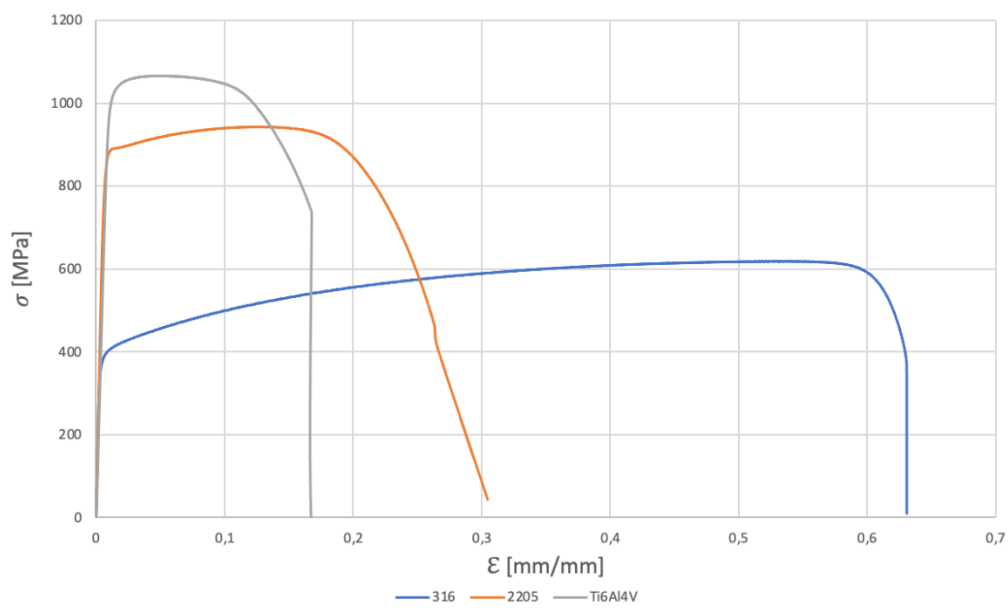

Figure 22 Thermocouple connected to the control unit

Table 10 Mechanical properties of the three materials

Properties	$Rp02\ [MPa]$	$R_m\ [MPa]$	$A\%$
AISI 316L	373	616,5	59,8
SAF2205	835	928	26,9
Ti6Al4V	989	1067	17

From the tensile curves obtained it is possible to see that titanium and duplex have a higher yield strength than AISI 316L. This is mainly due to the finer structure (specially for the titanium) and to the presence of alloying elements. As regards the elongation, AISI 316L is the material with greater elongation. Being austenitic, it has more systems and types of sliding due to twinning. Moreover, martensite is formed during the deformation and consequently a lot of energy is absorbed.

5.4 Fracture toughness test in air at room temperature results

In this section the results obtained for the fracture toughness tests in air at room temperature are summarized. Figure 46 presents the SE(B) specimens of each material after the tests.

| AISI 316L | SAF2205 | Ti grade 5 |

Figure 46 – SE(B) specimens after the fracture toughness tests.

Now for each material, a Force vs Displacement plot (P vs v), is represented (Figure 47, Figure 48 and Figure 49).
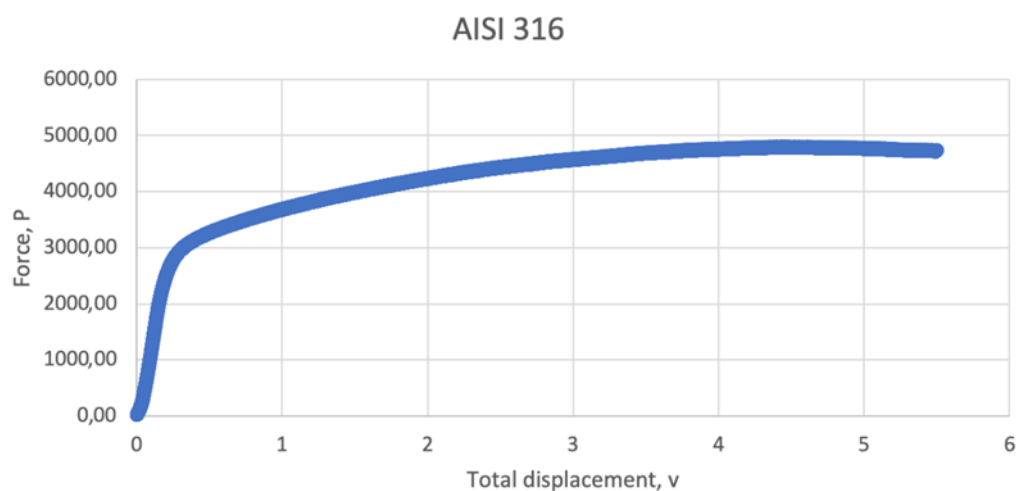

Figure 47 – Force *vs.* displacement record for the AISI 316L SE(B) specimen.
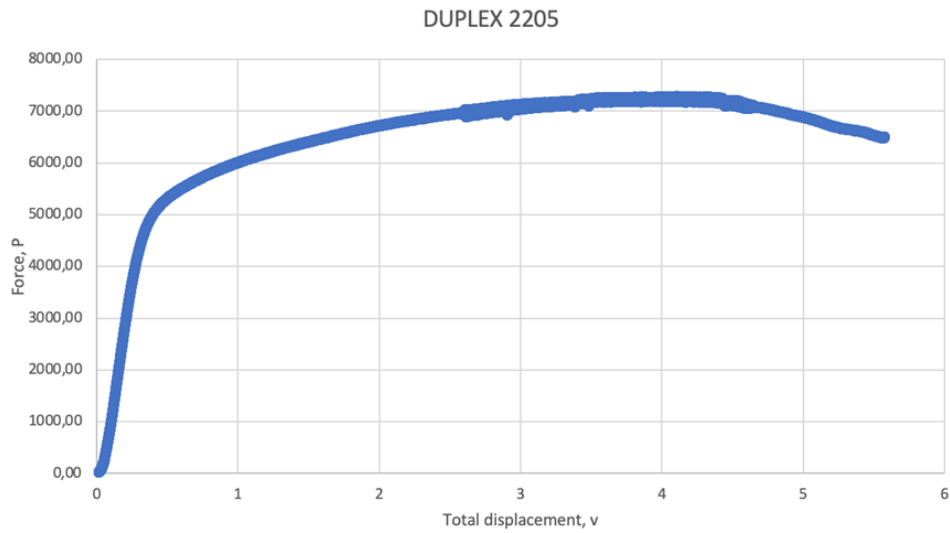
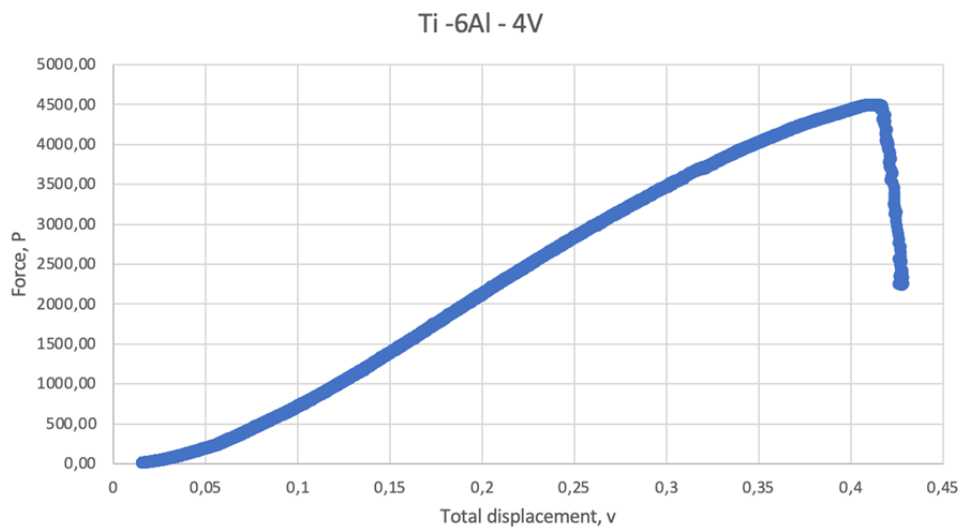Figure 48 – Force *vs.* displacement record for the SAF2205 SE(B) specimen.

Figure 49 – Force *vs.* displacement record for the Ti grade 5 SE(B) specimen.

From the *P vs.* displacement records, the *J*-integral values were calculated at the maximum load. Table 11 summarizes these values of *J* and the corresponding *K* values for the three SE(B) specimens of the three materials.

Table 11 Values of J and K derived from the fracture toughness test

Material	AISI316L	SAF2205	Ti6Al4V
$J\ [kJ/m^2]$	822,3	1243,5	38,8
$K\ [MPa\sqrt{m}]$	389,1	471,2	70,7

From the *P vs.* displacement records, it can be observed that the all SE(B) specimens for the three materials presented an elastic-plastic behaviour. However, AISI 316L and SAF2205 materials presented high levels of plastic deformation during the tests, while the SE(B) specimen of Titanium presented a significative instability at the beginning of the plastic regime. Those facts were quantitatively traduced by the fracture toughness values shown in Table 11. After the fracture toughness tests, a fatigue post–cracking procedure was performed, for the fracture surface analysis. Figure 50 and Figure 51 shows the fracture surfaces of the SE(B) specimens of AISI 316L and SAF2205 materials. In these images, the following regions are clearly seen: (a) the EDM notch, (b) the fatigue pre-cracked region, (c) the stable crack propagation region, (d) the post – cracking fatigue region, and (e) the cut surface.
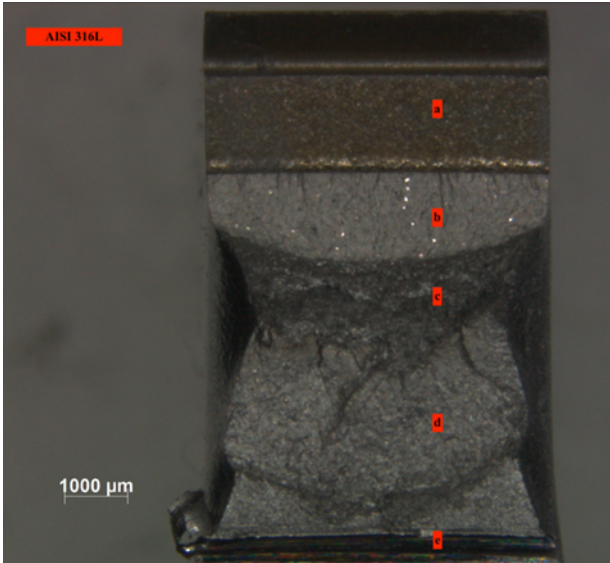
Figure 50 - Fracture surface of the AISI 316L SE(B) specimen.
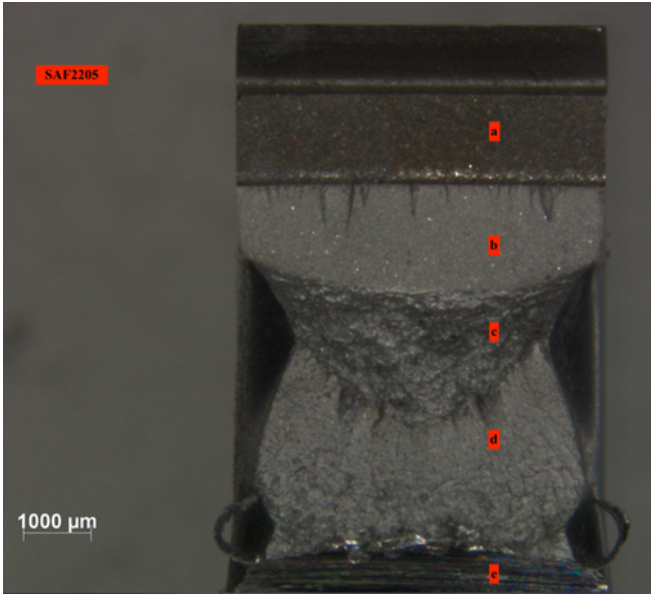
Figure 51 - Fracture surface of the SAF2205 SE(B) specimen.

For the SE(B) specimen of the Titanium Grade 5 material, the following regions are highlighted (Figure 52): (a) EDM notch, (b) fatigue pre-cracked, (c) instable crack propagation region, and (d) the fatigue post–cracked region.
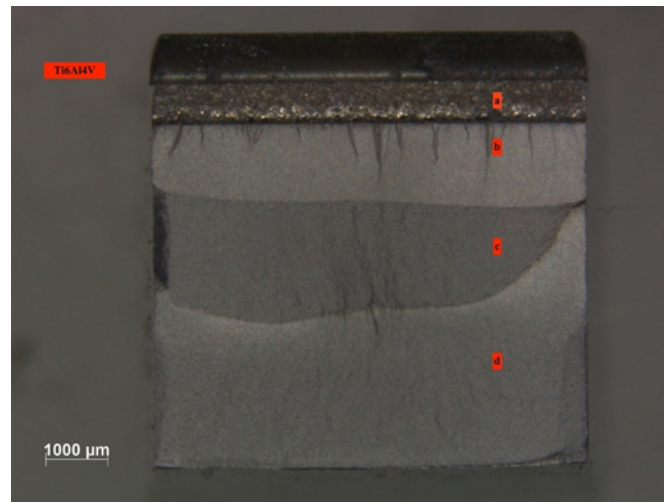
Figure 52 Fracture surface Ti grade 5 SE(B) specimen.

5.5 Results of the K_{ISCC} tests for rock anchors materials in marine environment

In this section, all the numerical results obtained in the K_{ISCC} test described in Section 4.6 are reported. The Table 12 summarizes the limiting values of K, derived with (16), and the applied K applied in each specimen. For conservativeness and to be sure that the stresses at the crack-tip were in the linear-elastic regime, the applied K values were lower than the limiting K ones.

Table 12 Limiting *K* values and the applied *K* ones.

K [$MPa\sqrt{m}$]	AISI 316L	SAF2205	SAF2205	Ti6Al4V	Ti6Al4V
K_{Limit}	28.0	62.2	62.4	56.3	57.3
K_{app}	22.0	48.0	45.0	45.0	48.0

In Table 13 there are reported the values of *P* [kN] derived with (18), the corresponding values in Volts obtained with (19) and the corresponding deformation $\mu\varepsilon$ evaluated for each specimen using (10), (11), (12), (13), and (14) equations.

Table 13 Values of load and deformation used for the test

	AISI 316L	SAF2205	SAF2205	Ti6Al4V	Ti6Al4V
$P[kN]$	1,84	4,00	3,79	3,24	3,65
P [V]	1,23	2,67	2,53	2,43	2,16
$\mu\varepsilon$ [$\frac{\mu m}{m}$]	334,51	-622,72	-551,77	487,68	470,39

After one month of load application at room temperature, the cracks do not propagate as can be seen by the Figure 53. In this figure, it can be seen all the deformation ($\mu\varepsilon/\varepsilon$) *vs* Time plot for each screw. As the deformation values remained in the same level, it can be inferred that the cracks do not propagate.
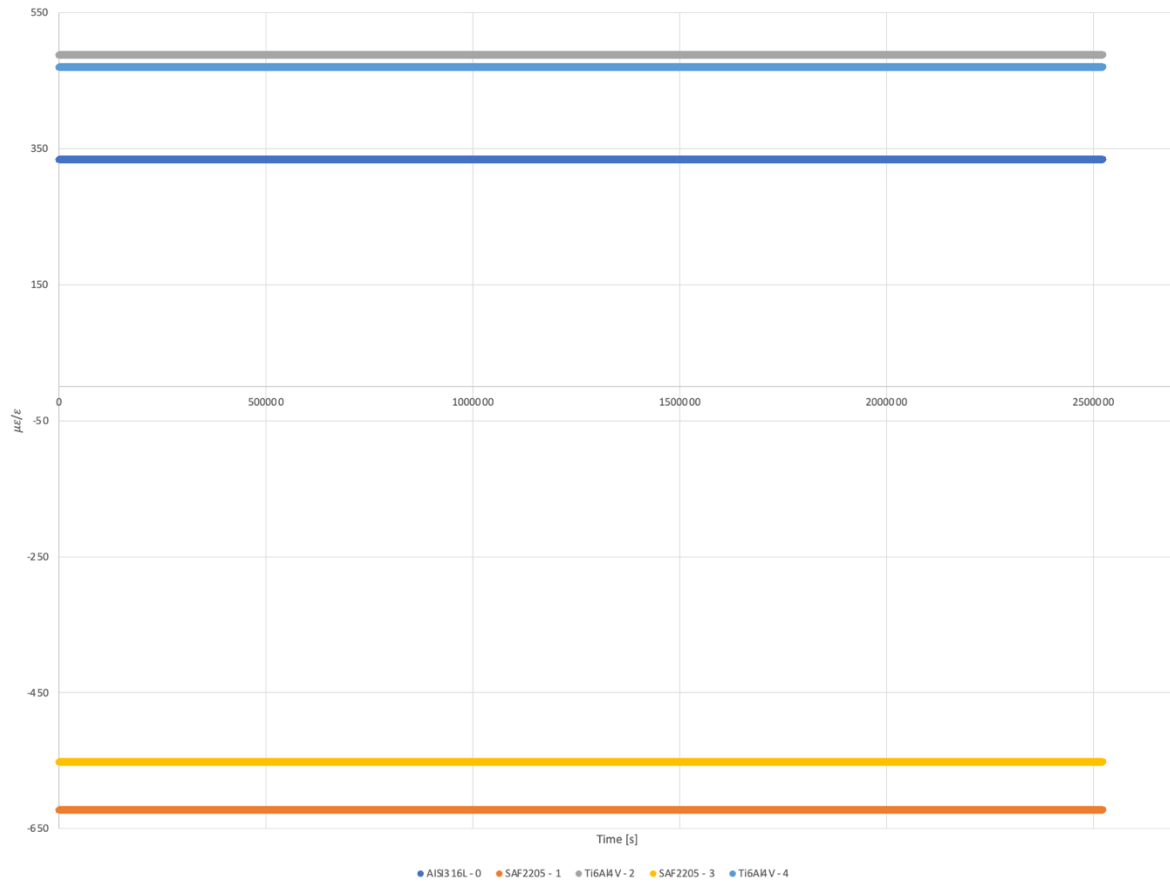
Figure 53 Deformation vs Time plot for each screw.

Figure 54 presents the temperature trend recorded during the entire duration of the test. Although there was a thermal variation for the entire duration of the test, the propagation of the cracks did not occur. As the cracks do not propagate during the experimental tests, the materials presented a good response for the *K* levels applied during the period of the tests.
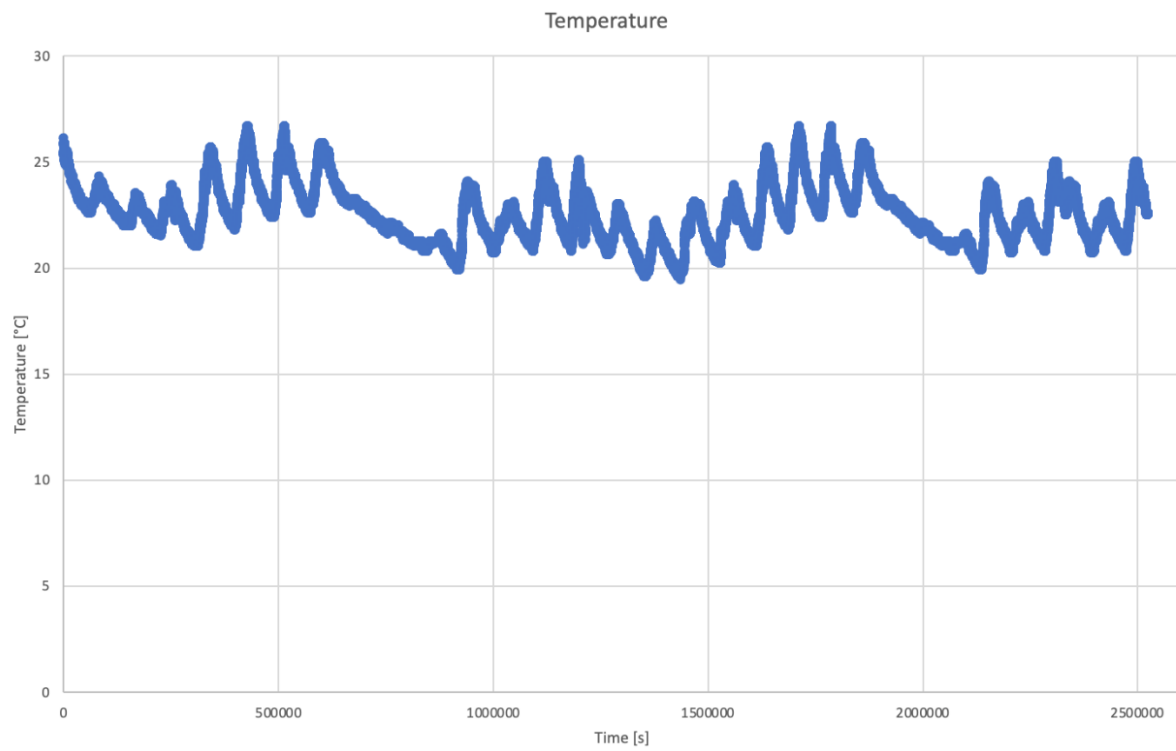
Figure 54 Temperature variations

6. Conclusions

The aim of this work was to define and propose a methodology useful to study the behavior of metal rock anchors under stress corrosion cracking conditions. The main topic was the failure of rock anchors in marine environment and, recognized the stress corrosion cracking as one of the main causes for failure, a test simulating this behavior was developed and performed on three different alloy (AISI316L, SAF2205 and Ti grade 5).

The setup was developed to carry out the test to determine the Keac by recreating the crack propagation under marine environment. The test is able to evaluate the variation of the load (in terms of deformation) over time, the yield rate, the maximum load and the behavior of the materials in selected conditions

The test has a good versatility, it allows to test the material under different loading conditions, different environments and temperature. This is particularly useful given the randomness of the environmental conditions where the anchors are installed.

After thirty days of test, no mechanical or chemical damage was found in the materials selected for loading condition close to K measured in air. This result testifies the goodness of the three alloy for this application in marine environment.

Bibliography

[1]   A. Gruttadauria, S. Barella, R. Gerosa, An overview of austenitic stainless – steel rock anchors damage in an environment rich with chlorides, 2019.

[2]   R. Schad, Analysis of climbing accidents, 1999.

[3]   D. G. Karalis, N. E. Melanitis, D. I. Pantelis, Failure analysis of a rock anchor made of stainless steel in marine environment, 2011.

[4]   UIAA 123 Rock Anchors, Climbing and Mountaineering Equipment, V4, December 2020.

[5]   J. Lieberzeit, T. Prošek, A. Jarvis, L. Kiene, Atmospheric Stress Corrosion cracking of Stainless Steel Rock Climbing Anchors, Part 1, 2019.

[6]   T. Prošek, J. Lieberzeit, A. Jarvis, L. Kiener, Atmospheric Stress Corrosion Cracking of Stainless Stee Rock Climbing Anchors, Part 2: Laboratory experiments, 2019.

[7]   A. Sjong, L. Einstein, Marine atmospheric SCC of Unsensitized stainless steel rock climbing protection, 2008.

[8]   B. R. Khatak, Corrosion of austenitic stainless steel, Woodhead publishing, 2002.

[9]   Staehle, The theory of stress corrosion in alloys, J. C. Scully, 1971.

[10]   T. L. Anderson, Fracture Mechanics – Fundamentals and applications, Third edition, Taylor & Francis, 2005.

[11]   R. P. Wei, Fracture Mechanics – Integration of mechanics, materials science and chemistry, Cambridge, 2010.

[12]   S. Barella, A. Gruttadauria, Metallurgia e materiali non metallici, 2016.

[13]   ASTM E399-20a, Standard Test Method for Linear-Elastic Plane-Strain Fracture Toughness of Metallic Materials, ASTM International, West Conshohocken, PA, 2020.

[14]   ASTM E1820-20, Standard Test Method for Measurement of Fracture Toughness, West Conshohocken, PA, ASTM International, 2020.

[15]   ASTM G36-94 (2018), Standard Practice for Evaluating Stress-corrosion Cracking Resistance of Metals and Alloys in a boiling Magnesium Chloride Solution, West Conshohocken, PA, ASTM International, 1994.

[16]   ASTM B117-19, Standard Practice for Operating Salt Spray (Fog) Apparatus, West Conshohocken, PA, ASTM International, 2019.

[17]   AA. VV, ASM Handbook vol. 9: Metallurgy and Microstructures, ASM Int. Mater, Park. OH, 2004
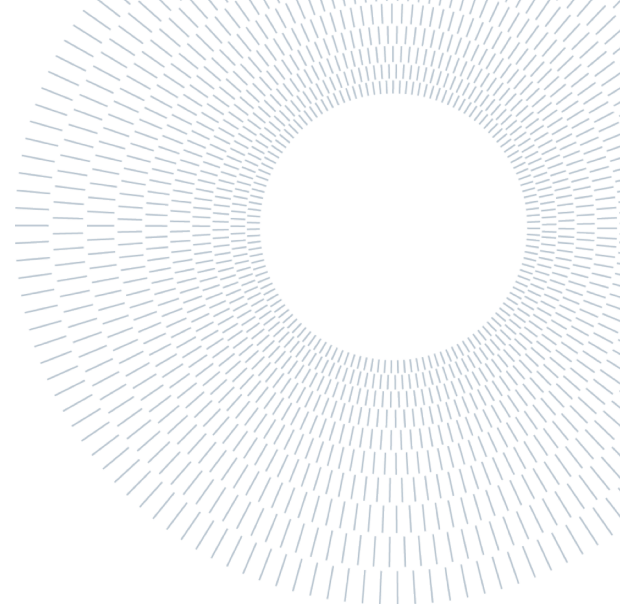
Acknowledgements

For the editing of this paper and the opportunity of taking part in this thesis research, a special thanks goes to professors Ing. Andrea Gruttadauria, Prof.ssa Silvia Barella and to Ing. João Teixeira Oliveira de Menezes.

EXECUTIVE SUMMARY OF THE THESIS

Methodology for the determination of the K_{ISCC} for rock anchors materials in marine environment

TESI MAGISTRALE IN MATERIALS ENGINEERING AND NANOTECHNOLOGY – INGEGNERIA DEI MATERIALI E DELLE NANOTECNOLOGIE

AUTHOR: GIUSEPPE CARISTO

ADVISOR: ANDREA GRUTTADARIA

ACADEMIC YEAR: 2020-2021

1. Rock anchors for sport climbing

Sport-climbing has become an increasingly popular sport since the '80s, when the first pioneers laid the foundations of this fun activity. The increasing number of people approaching climbing, led to an increment of the so-called world climbing destinations; on the other hand, with the growth of seaside climbs around the world, there has been an increasing number of accidents related to anchor failures.

1.1 Type of bolts

Basically two types of climbing anchors [1] exist: Glue – in bolts and expansion bolts. Glue – in bolts are recognized as the most durable bolts used in rock climbing today. This kind of bolt are essentially a piece of high – grade bar stock glued into a drilled hole with construction grade epoxy. They can vary slightly in shape and composition, but all of this type of bolt have in common a ring on one end for clipping. Having no metal on metal

contact or moving parts and largely encased in a waterproof epoxy, they resist corrosion more than any other bolts. On the other hand, these bolts are perhaps the most difficult to be placed. Glue – in bolts are available in 304 and 316 stainless steel, while for particularly corrosive environments they are made of titanium. Most glue – in bolts are placed in a hole drilled slightly larger than the diameter of the bolt itself; this allows the epoxy to encase the bolt, forming in this way a reliable bond with the rock. Expansion bolts (Figure 1) are the widest installed bolts because of their low cost and easiness of installation, if made by stainless steel they can last several decades also in aggressive environments. They consist of a threated bolt with a single or double conical end wrapped in a clip. A nut and a washer are attached to the threated end. This kind of bolt is installed being hammered into a properly sized hole and as it is tightened the cone pulls forward causing the clip to grip inside the hole.
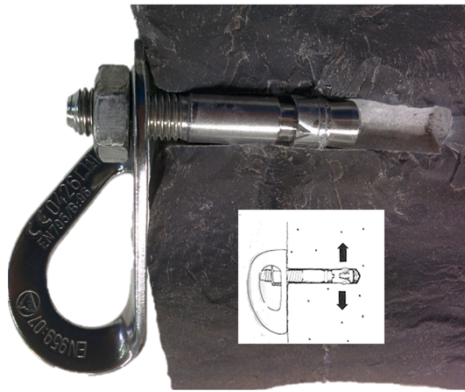
Figure 1 Expansion bolt

To place this type of bolt, first a hole needed to be drilled in the rock (diameter of the drill equal to the diameter of the bolt); the hole must be perpendicular to the rock and in a flat area; an air pump is required in order to remove the dust from the hole and finally the bolt can be hammered.

1.2 Failure of rock anchors

The presence of corrosive environment, the tightening induced stresses and the susceptibility of the anchor material to stress corrosion cracking are the most critical parameters that may influence the life of the anchor [3].

Figure 2 Example of rock anchor failure

One of the main causes of the failure of rock anchors in marine environments is stress corrosion cracking [4] and there are some factors contributing to this problem [6]: concentration of chlorides, temperature, humidity, position in respect to the sea and rock type.

Stress corrosion cracking is the considered phenomenon responsible for the failure of the anchors analysed (Figure 3).
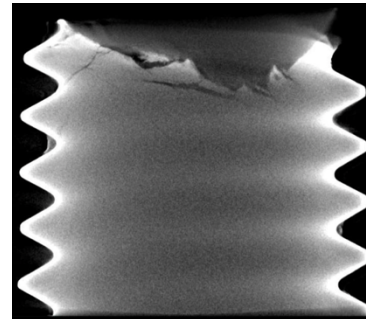

Figure 3 Climbing bolt under SCC

The material failure is accelerated by the combined effect of corrosion and mechanical stress and eventually temperature [8]. An important factor that has to be evaluated in order to characterize this form of corrosion and its effect, in this particular case, on rock anchors, is the K_{EAC}: the stress intensity factor necessary to propagate a crack by the SCC phenomenon. This parameter depends on the material composition and the environment. The knowledge of this parameter is important for the structural integrity of components that operate in similar conditions of the tests. Stress corrosion cracking (SCC) is considered as a problem of long standing. It manifests itself as a *delayed failure* [11] mode: a failure which occurs after some period of time of structural component under statically applied loads, at stresses well below the yield strength of the material. The traditional measure used for stress corrosion cracking susceptibility is given in terms of the time necessary to produce failure at different stress levels, obtained from testing smooth or notched specimens of the material in corrosive environment, for example in sea water for marine applications. From the design and engineering perspective using the fracture mechanics parameters and concepts, it is important to focus on the determination of a threshold stress intensity factor that would provide some safety conditions over the service-life of the component or structure. In particular, for the SCC phenomenon, the K_{ISCC} and crack growth rate (da/dt). The UIAA 123 (2021) is the referring standard for mountaineering equipment; this standard proposes two different tests for rock anchors ASTM G36 and ASTM B117:

- According to ASTM G36 – 94: This practice describes a procedure for conducting stress-corrosion cracking tests in a boiling magnesium chloride solution. Although this test may be performed using various

concentrations of magnesium chloride, this procedure covers a test solution held at a constant boiling temperature of 155.0 6 1.0°C (311.0 6 1.8°F). The boiling magnesium chloride test is applicable to wrought, cast, and welded stainless steels and related alloys. It is a method for detecting the effects of composition, heat treatment, surface finish, microstructure, and stress on the susceptibility of these materials to chloride stress corrosion cracking. The duration of this test indicated in UIAA 123 is about one week;

- According to ASTM B117: This practice covers the apparatus, procedure, and conditions required to create and maintain the salt spray (fog) test environment. The apparatus required for salt spray (fog) exposure consists of a fog chamber, a salt solution reservoir, a supply of suitably conditioned compressed air, one or more atomizing nozzles, specimen supports, provision for heating the chamber, and necessary means of control. The duration of this test indicated in UIAA 123 is about four weeks.

The first experimental procedure described considers the resistance to pitting which will certainly be high for the proposed materials, due to the presence of Mo for AISI 316L and SAF2205, and the non - susceptibility for the Titanium Grade 5. This test is based only on the presence of sprays and as described in several studies [1], the condition for having pitting from which to start the cracks are many and all almost independent of the presence of chlorine.

The other procedure, on the other hand, distorts the conditions with a corrosion that is too aggressive (but which explains the reason for only one week of testing), however not taking into account the presence of notch that derives from the pit (generated as mentioned by different conditions) and not thus offers an idea of the applied loads; with the proposed test instead, it is possible to record these loads and relate them to the properties of the materials. At this point, this work wants to propose a methodology that also takes into consideration the resistance of the materials: through the determination of K_{ISCC} taking into consideration the corrosive environment, the presence of the notch (recreating

the pitting condition) and through controlled loading conditions.

2. Materials and methods

The experiment was conducted on three different alloy which are respectively two stainless steel (austenitic grade AISI 316L and duplex SAF2205) and Ti alloy grade 5.

2.1 Materials characterization

First of all, according with the procedure is given by ASM Metal Handbook Volume 9 "Metallography and microstructure", some samples of the three materials have been prepared in order to analyse the microstructure (polishing and etching); then, some hardness test have been performed, following the standard ASTM E 18 - 07 for the Rockwell and ASTM E92 – 17 for the Vickers; then, according to the standard ISO 6892 a tensile test in order to obtain the mechanical properties of the materials have been performed, with a speed of 2 mm/min.

3. Specimen fracture analysis and test

In this section there are described the geometry of the specimens and the different procedures carried out in order to prepare the specimens for the final test, which consist in a constant displacement test in marine environment (synthetic seawater 3,5 % NaCl).

3.1 Specimen type and geometry

According to ASTM E1820 and ASTM E399, the specimen selected for the test is the SE(B) type: this standard bend specimen is a single – edge – notched and fatigue – cracked beam loaden in three point – bending with a support span, S, equal to four times the width, W. Samples were taken from the center of cold drawn bars. This is because this type of semi-finished products (or laminates) are mainly used to make the anchors and which in any case have a microstructure similar to that of the anchors.

3.2 Fatigue pre – cracking

Before starting the tests, the specimens described before must be prepared; in particular, according to ASTM E1820, it is necessary to fatigue pre-crack the specimens using three point – bending methods. Through a visual inspection during and after the pre-cracking phase, the length of the crack reached was of 1mm, obtaining in this way a characteristic length a_f. In table 1 there are resumed the crack lengths.

Table 1 Crack lengths

Material	AISI 316L	SAF2205	Ti6Al4V
a_i [mm]	2,5	2,5	1,5
Crack length [mm]	1	1	1
a_f [mm]	3,5	3,5	2,5

3.3 Fracture toughness test in air at room temperature

According to ASTM E1820-18 a fracture toughness test in air at room temperature was performed, in order to evaluate the fracture toughness for the materials considered, in particular evaluating K and J. For the single edge specimen, the parameter J was calculated as follow:

$$J = \frac{K^2 (1 - \nu^2)}{E} + J_{pl} \tag{1}$$

Where in particular:

$$K_{(i)} = \left[\frac{P_i S}{(BB_N)^{1/2} W^{3/2}}\right] f\left(\frac{a_i}{W}\right) \tag{2}$$

and
$$J_{pl} = \frac{\eta_{pl} A_{pl}}{B_n b_0} \tag{3}$$

These two parameters (whose values are reported in chapter 4) allow to have an idea of the fracture toughness and of the elastic and plastic behavior of the different materials.

3.4 Equipment preparation

In this study, the three – point bending test was performed and analysed: each specimen is placed inside a structural frame (Figure 4), which was in a previous step covered with an anti – rust spray and

is standing on two rollers; the compression is given by the calibrated and connected with extensometers screw through a metallic sphere.
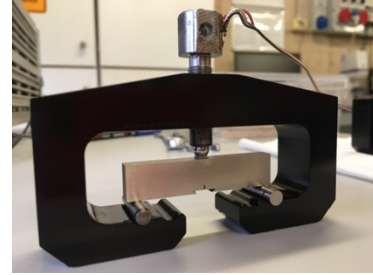

Figure 4 Specimen placed inside a frame

Each frame is then put into a 3.5% wt NaCl solution, used to simulate sea water. Each screw is tightened according to the load to be applied. The extensometers fixed inside a hole drilled in each screw (Figure 4) measure the deformation of the screw itself related to the compression and to the load applied into each specimen; all the acquired data are then recorded and analyzed through an electric control unit. Due to the fact that the load applied to each specimen through the screw is read from the control unit in terms of deformation (μm/m), a proper calibration of each screw is needed. The purpose of this calibration test is to obtain a linear Strain vs Load plot and an equation for each screw. In this way, knowing the loads needed to be applied, converting them from kN to V, it is possible to derive the corresponding deformations.

3.5 Experimental test description

For the test, five frames with five calibrated screws are prepared; they are put inside a propylene box immersed in the solution. Before starting with the test, different stages are required in order to prepare all the equipment. At first, the maximum K relative to the limit for the elastic behavior for each specimen is calculated, according to ASTM E1681 through the following equation:

$$K = \sigma_{ys}\sqrt{\frac{\pi b_0}{4}} \tag{5}$$

Then, once the maximum values of K have been calculated, lower values of K are chosen for each specimen, in order to have a more conservative approach and in order to be sure of being in the elastic range and also because the aim of this work is to find a threshold value (K_{ISCC}). These value of K are also important because they corresponds to

the load, and as a consequence, to the deformation applied on each specimen tightening each screw; in particular, according to ASTM E1820,it is possible to derive the load applied on each screw (kN):

$$P = \frac{K(BB_N)^{1/2}W^{3/2}}{S\, f\left(\frac{a}{W}\right)} \qquad (6)$$

Once the loads have been calculated, they must be converted from kN to V, using (4); At this point, having all the loads in Volts, it is possible, using the equation obtained from the calibration phase, deriving for each specimen its proper deformation ($\mu\varepsilon$) which is the parameter read from the control unit and corresponding to the load applied in each specimen. Then, each specimen is placed in its frame and the relative load was applied by tightening each screw until reaching the corresponding value, reading the corresponding deformation from the control unit. At this point each frame is placed inside the PP box with the solution and the test starts (Figure 5).

Figure 5 Specimen immersed in solution

In order to control also the temperature variation during day, night and weekend, a thermocouple was connected to the control unit.

4. Results

In this section, the main results obtained from the test described in previous sections are reported. The microstructures, the hardness and the mechanical properties obtained are consistent with the three materials and with the thermomechanical treatments. In table 2 there are reported the mechanical properties obtained during tensile test.

Table 2 Mechanical properties of the materials

Properties	$Rp02\ [MPa]$	$R_m\ [MPa]$	$A\%$
AISI 316L	373	616,5	59,8
SAF2205	835	928	26,9
Ti6Al4V	989	1067	17

After the fracture toughness test in air at room temperature, values of J and K for each material have been obtained and they are summarized in Table 3.

Table 3 Values of J and K

	AISI 316L	SAF2205	Ti6Al4V
J $[kJ/m^2]$	822,3	1243,5	38,8
K $[MPa\sqrt{m}]$	389,1	471,2	70,7

In Table 4 there are summarized the values of K max, derived with (5), and of K applied for each specimen.

Table 4 Values of K derived and used during the test

$K\ [MPa\sqrt{m}]$	316L	SAF2205	SAF2205	Ti6Al4V	Ti6Al4V
MAXIMUM	28,0	62,2	62,4	56,3	57,3
APPLIED	22	48	45	45	48

In table 5 there are reported the values of P [kN] derived with (4), and the corresponding deformation $\mu\varepsilon$ evaluated for each specimen using the equations obtained from the calibration phases.

Table 5 Loads and deformations

	316L	SAF2205	SAF2205	Ti6Al4V	Ti6Al4V
$P[kN]$	1,84	4,00	3,79	3,24	3,65
$\mu\varepsilon\ \left[\frac{\mu m}{m}\right]$	334,51	-622,72	-551,77	487,68	470,39

After a month of loads application at room temperature, in Figure 6there are represented all the Deformation ($\mu\varepsilon/\varepsilon$) vs Time plot for each screw:
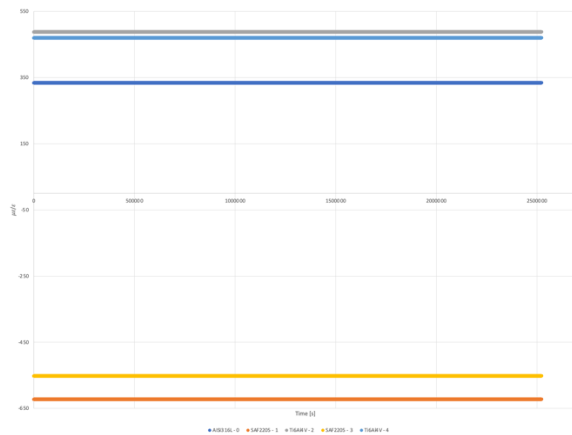
5

Figure 6 Deformation vs Time plot

As it is possible to see, the deformation values for each screw remain all the same. In Figure 7 there is represented the temperature trend recorded during the entire duration of the test.
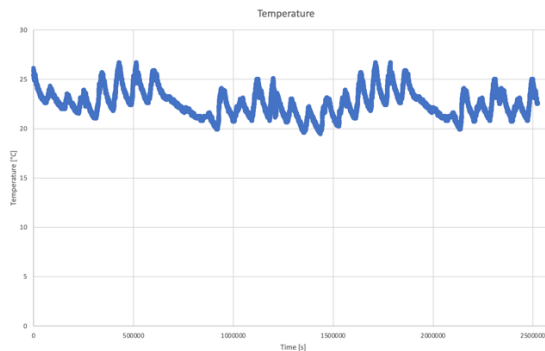

Figure 7 Temperature variations

Although there was a thermal variation for the entire duration of the test, the propagation of the crack did not occur in the specimens. There was no mechanical alteration in the three materials which therefore, for the duration of the test and under the established conditions, had a good behavior in the intended application.

5. Conclusions

The aim of this work was to define and propose a methodology useful to study the behavior of metal rock anchors under stress corrosion cracking conditions. The main topic was the failure of rock anchors in marine environment and, recognized the stress corrosion cracking as one of the main causes for failure, a test simulating this behavior was developed and performed on three different alloy (AISI316L, SAF2205 and Ti grade 5).
The setup was developed to carry out the test to determine the K_{ISCC} by recreating the crack

propagation under marine environment. The test is able to evaluate the variation of the load (in terms of deformation) over time, the yield rate, the maximum load and the behavior of the materials in selected conditions
The test has a good versatility, it allows to test the material under different loading conditions, different environments and temperature. This is particularly useful given the randomness of the environmental conditions where the anchors are installed.
After thirty days of test, no mechanical or chemical damage was found in the materials selected for loading condition close to K measured in air. This result testifies the goodness of the three alloy for this application in marine environment.

References

[1] Andrea Gruttadauria, Silvia Barella, Riccardo Gerosa, An overview of austenitic stainless – steel rock anchors damage in an environment rich with chlorides, 2019.

[2] D. G. Karalis, N. E. Melanitis, D. I. Pantelis, Failure analysis of a rock anchor made of stainless steel in marine environment, 2011.

[3] UIAA 123 Rock Anchors, Climbing and Mountaineering Equipment, V4, December 2020.

[4] Tomáš Prošek, Jiří Lieberzeit, Alan Jarvis, Lionel Kiener, Atmospheric Stress Corrosion Cracking of Stainless Stee Rock Climbing Anchors, Part 2: Laboratory experiments, 2019.

[5] B. R. Khatak, Corrosion of austenitic stainless steel, Woodhead publishing, 2002.

[6] Robert P. Wei, Fracture Mechanics – Integration of mechanics, materials science and chemistry, Cambridge, 2010.

Acknowledgements